Chapter 2
O_2 Analysis on a Fluorescence Spectrometer or Plate Reader

Alexander V. Zhdanov, James Hynes, Ruslan I. Dmitriev and Dmitri B. Papkovsky

Abstract In this chapter, the use of Pt-porphyrin-based extracellular and intracellular O_2 sensing probes (ecO_2 and icO_2) on a TR-F plate reader format is described and critically assessed. The principles underpinning extracellular measurement are outlined and the assessment of biological oxygen consumption in prokaryotic cells, eukaryotic cells and small organisms is outlined along with a description of how such measurements can contribute to the development of a detailed picture of cell metabolism. The use of a mathematical model describing the distribution of local O_2 gradients within biological samples is also described. Finally, the principles of icO_2 sensing are discussed and some short case studies are provided for demonstrating the utility of icO_2 probes for the monitoring of cellular function and metabolic perturbations and how such measurements can be allied to other bioenergetic markers to generate a more complete picture of metabolic status.

Keywords Oxygen · Respiration · Cell-based assays · Phosphorescent Probes · Pt-porphyrins · Time-Resolved Fluorescence · Oxygen-Sensitive Probes · Screening

2.1 Introduction

As outlined in Chap. 1, the simplest approach to the assessment of biological O_2 consumption by luminescence quenching is to introduce an O_2-sensitive material (a dispensable probe [1] or a solid-state sensor [2]) into the medium surrounding of the test specimen, measure its luminescent signal on a conventional fluorescence spectrometer or plate reader and then relate this signal to O_2 concentration or consumption rate (OCR). Extracellular O_2 (ecO_2) probes allow simple, parallel OCR

D. B. Papkovsky et al., *Phosphorescent Oxygen-Sensitive Probes*, SpringerBriefs in Biochemistry and Molecular Biology,
DOI: 10.1007/978-3-0348-0525-4_2,

measurement in multiple samples facilitating the assessment of metabolic impact of biological processes such as cell transformation genetic manipulation, drug treatment or culture conditions. Measurements are typically performed on adherent or suspension cell populations in microplate format. The method can also be applied to other specimens including aquatic organisms and model animals (such as *C. elegans*, *Artemia*, *Zebrafish*, *Daphnia)* [3, 4], and on more specialised measurement formats such as customised microplates [5], capillary cuvettes [6] or fluidic biochips [7].

For specific research questions, information on the O_2 concentration within the cell rather in the medium surrounding the cell can be particularly informative and provide a different insight into cellular function [8]. This can be achieved using *intracellular* O_2 (icO_2) probes representing (macro)molecular [9] or nano-particulate [10] structures delivered into the cell either by means of commercial transfection reagents [11], microinjection or by self-loading via endocytosis pathways [10, 12–14]. The latter approach relies on cell-penetrating O_2 probes supersedes the other strategies due to its convenience, reproducibility and efficiency. Optical measurements with loaded cells can be conducted over several hours [15], allowing for real-time monitoring of cell oxygenation levels at different conditions and levels of atmospheric O_2, and of rapid transient respiratory responses to cell treatment [16, 17].

Both techniques are simple, contactless, quantitative and facilitate high-throughput plate reader-based analysis of OCR or icO_2, providing useful and physiologically relevant information on cellular function. The optical detector interrogates the probe from outside the sample making these platforms flexible and non-invasive. Best performance is achieved when using high-sensitivity multi-label time-resolved fluorescence (TR-F) readers in lifetime measurement mode such as RLD (see Chap. 1). Such instruments are produced by a number of vendors (e.g., FLUOstar and POLARStar Omega® instruments from BMG Labtech GmbH, Germany and the Victor® family from PerkinElmer, USA), they are available in many life sciences labs and can be used without major modifications with several existing Pt-porphyin-based O_2 sensing probes (also produced commercially). These instruments also allow for multiplexed and parallel use of O_2 probes with other compatible probes and assays [18].

While the imaging-based measurements (outlined in detail in Chap. 3) offer considerable information on intracellular oxygen facilitating single cell detalisation and high-resolution 2D and 3D O_2 mapping, such systems suffer from some drawbacks with regard to sample throughput and a requirement for more sophisticated, often custom-modified equipment. In contrast, plate-reader-based O_2 analysis can facilitate intracellular analysis with much higher sample throughput using less sophisticated broadly available instrumentation, albeit at the expense of a degree of detail.

In this chapter, we describe the various uses of Pt-porphyrin-based extracellular and intracellular O_2 probes, in conjunction with plate-reader-based analysis across various biological systems. A significant number of applications developed in our lab and experimental studies performed in collaboration with academic and industrial partners are presented. Critical technical considerations are outlined, the potential for parallel measurements with other added-value techniques is explained

in detail, with the aim of providing the reader with a more comprehensive understanding of the capabilities and limitations of these technologies and a guide as to how to apply these techniques in their own research.

2.2 Bioassays Performed with ecO$_2$ Probes

Extracellular probes are typically deployed in the test medium and report on the rate at which biological O_2 consumption depletes the O_2 concentration within the sample. When devising an appropriate set-up for such measurements, the two main considerations are the OCR within the sample and the rate at which ambient O_2 diffuses back into the system. The most convenient format for such analysis is the standard microtiter plate. This approach can be applied to any test system which produces a detectable level of O_2 consumption with examples including isolated mitochondria [19], enzymes [6], yeast and prokaryotic suspensions [20], adherent eukaryotic cells [21], spheroids and small aquatic organisms [4]. The dissolved O_2 gradient generated while O_2 is consumed within the well drives the diffusion of ambient O_2 into the sample at both the liquid–air interface and through the body of the microplate (common plastic materials such as polystyrene are rather permeable to O_2). Measurement, therefore, usually necessitates the use of a seal, often a mineral oil overlay, to slow such back diffusion. After an equilibration phase, either a steady state is reached or all available O_2 are depleted.

The flexibility associated with ecO$_2$ probes also facilitates measurements in instances where the amount of analysed biomaterial is limited. This is achieved through the use of narrow bore glass capillaries where high sensitivity measurement can be conducted in volumes as low as several microliters [6], and further volume reduction is possible using specially designed devices made of O_2-impermeable materials [5, 7]. The capillary cuvette provides considerable sensitivity due to the limited surface area available and thick barrier of liquid for O_2 back diffusion and can be applied to the analysis of multiple samples on the commercial LightCycler® system [6] which was originally developed for quantitative PCR. Ground capped quartz or glass cuvettes provide hermetic seal which prevents the ingress of ambient O_2 and allows accurate and sensitive O_2 analysis on a TR-F reader or even intensity-based spectrometer, as outlined in Chap. 1 (Fig. 1.5).

2.2.1 Analysis of Isolated Mitochondria

One of the areas, where the use of phosphorescence based ecO$_2$ probes have seen widespread adoption, is in the assessment of mitochondria activity, specifically as a high-throughput method of analysing the metabolic implications of drug treatment. OCR measurements are favoured in this regard as they assess directly the

activity of the electron transport chain (ETC) and are, therefore, highly sensitive to perturbations in mitochondrial function. Much of this work is conducted on the organelles isolated from rat liver or heart and, as with any organelle-based assays, a key parameter is the quality of the mitochondrial preparation [19, 22]. These measurements are particularly useful where mechanistic information is sought on the mode of action of the mitochondria perturbation as it assures free access of the compound to the machinery of the mitochondria, removing the possible complications with transportation across cell membrane. Detailed mechanistic investigations can be achieved through the use of substrates which feed reducing equivalents to specific complexes along the ETC.: glutamate/malate, succinate and ascorbate/TMPD (N,N′,N′,N′-tetramethyl-p-phenylenediamine) for complexes I, II and III, respectively. Fatty acid oxidation pathway can also be probed through the use of palmitate as a substrate.

Traditionally, such analyses were achieved using standard polarography, however, limited throughput has restricted this adoption. The necessary throughput is achieved using a water-soluble O_2 probe on a standard microplate format [19], which allows for the generation of dose response data and analysis of multiple substrates in both the presence and absence of ADP. Sample data are presented in Fig. 2.1 illustrating phosphorescence intensity profiles which reflect O_2 profiles and OCRs produced by the samples of rat liver mitochondria. Measurement in the presence of ADP allows the detection of inhibitors of ETC function as seen by the antimycin A (Ant A) treatment in Fig. 2.1a, while rotenone, a potent complex I inhibitor does not cause inhibition as succinate is the substrate feeding reducing equivalents via complex II and bypassing the site of inhibition. Rotenone does, however, show inhibition where glutamate/malate are substrates (Fig. 2.1b) as in this instance, reducing equivalents are fed through complex I. Measurements in Fig. 2.1b are conducted in the absence of ADP allowing the detection of uncoupling as shown by FCCP treatment. Such measurements can also be used to assess the involvement of the mitochondrion in various disease states [23, 24].

2.2.2 Analysis of Mammalian Cell Respiration

While analysis in the isolated organelle is particularly advantageous in specific circumstances, for many applications it is preferable to assess mitochondrial function within the whole cell, where it is fully integrated with the various secondary metabolic controls and regulatory mechanisms while also ensuring the integrity of the cellular ultrastructure and related signalling. There has been a growing realisation over recent years of the importance of this integration, to the extent that mitochondria are no longer considered as unifunctional free standing organelles but as a complex dynamic reticulum [25]. It is clear, therefore, that cell-based assessment of mitochondrial function is of particular importance, especially for the studies of the compounds or treatments that obstruct oxidative metabolism. However, many standard assays measure end-points which are secondary to the

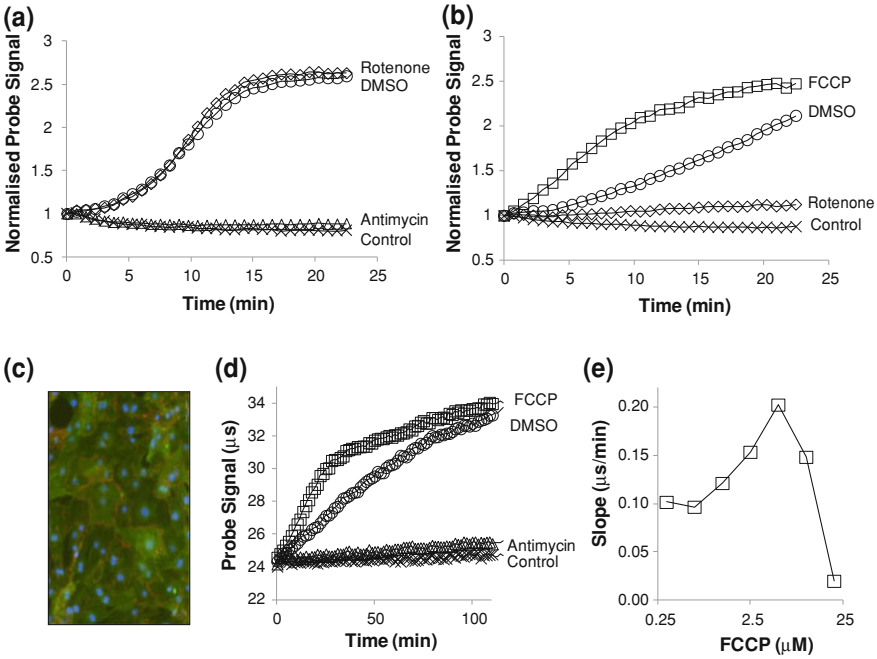

Fig. 2.1 Respiration profiles for isolated mitochondria (**a**, **b**) and whole cells (**d**, **e**) measured with the ecO_2 probe MitoXpress®. **a** Normalised intensity profiles for isolated mitochondria on Succinate in the presence of ADP showing ETC inhibition. **b** Isolated mitochondria on Glutamate/Malate in the absence of ADP showing ETC inhibition and uncoupling. **c** Immunofluorescence of Cor.At mESC derived cardiomyocytes demonstrating s-actin (*green*) contractile filaments and connexin 43 (*orange*) gap junctions between cardiomyocytes. **d** Lifetime-based respiration profiles of Cor.At cell showing both ETC uncoupling and inhibition (Ant A). **e** FCCP dose response whereby an initial increase in OCR is followed by a significant reduction in ETC activity caused by non-specific cell damage. Image used with permission from Axiogenesis AG (Germany)

activity of the mitochondria. Under standard culture conditions, many cell lines exhibit the capacity to maintain cellular ATP supply via increased glycolytic flux despite the complete shutdown of oxidative phosphorylation (OxPhos) metabolism, a phenomenon termed the Crabtree effect [26]. In such instances, if secondary parameters, such as ATP, or the reductive capacity of the cell as measured by MTT or Alamar blue assays, are taken as an indication of mitochondrial health, this can lead to a considerable underestimation of the level of metabolic inhibition [26]. For this reason, direct OCR measurement is particularly valuable as it facilitates a direct analysis of the mitochondrial function and is not susceptible to such misinterpretation. OCR measurement in whole cells is conducted in a manner similar to that used for isolated mitochondria where the rate of O_2 depletion within the sample is monitored over time [21].

The ability to interrogate mitochondrial function while maintaining cellular ultrastructure and related signalling is evident in the assessment of stem cell-

derived cardiomyocytes. Such cell cultures are often favoured over primary cells as they circumvent the isolation and purity difficulties often associated with primary cells. Figure 2.1c–e illustrates the measurement of relative OCR for Cor.At cardiomyocytes (Axiogenesis AG, Germany), which are produced from mouse embryonic stem (ES) cells through in vitro differentiation and, similar to primary cells, have limited proliferative capacity. These cells exhibit a high energy demand, express functional cardiomyocyte ion channels and receptors, and a stable beating signal. They are puromycin resistant thereby allowing the generation of a homogenous and reproducible cell system [27]. Their ultrastructural complexity is illustrated in Fig 2.1c, showing cells after a 4 week culture period with s-actin stained green, highlighting the contractile filaments and Connexin 43 stained orange demonstrating gap junctions between cardiomyocytes. The metabolic impact of compounds known to inhibit electron transport chain function is presented in Fig. 2.1d, where both Ant A and the FoF1 ATP synthase inhibitor oligomycin induce an immediate inhibition of OCR. In contrast, treatment with FCCP causes an uncoupling related increase in OCR, the associated dose–response relationship is presented in Fig. 2.1e. Cellular OCR increases until a critical FCCP concentration is reached after which point, OCR declines due to cell damage.

This type of analysis with ecO_2 probes has been applied to many cell types including primary neurons [28], primary rat hepatocytes [21], myoblasts [29], cancer cells [30] and examining phenomena such as pharmacological perturbation of the ETC. activity [31], genetic modulation of ETC complexes [32] and the role of PGC-1α and PNC1 in mitochondrial biogenesis and function [29, 30]. This approach has also been perused as a diagnostic tool for the evaluation of suspected mitochondrial disorders using digitonin permeabilised patient-derived fibroblasts. Permeabilisation allows direct access of compound or substrate to the mitochondrial network facilitating an analysis of the entire OxPhos apparatus in whole cells and allowing comparison with data from human-derived isolated mitochondria. Such a comparison aids the differentiation of primary and secondary mitochondriopathies. This approach is also applicable to the screening of cybrid clones for mitochondrial dysfunction related to mtDNA mutation [33].

Despite advances in the development of biological models such as those described above, the standard 2D cultured cells still lack the biological complexity necessary to investigate certain biochemical processes. This is particularly relevant in tumour biology where the tumour microenvironment often contains hypoxic regions which are thought to be relevant to tumour aggressiveness and response to particular therapies. Multi-cellular spheroids offer an alternative to 2D cultures for the investigation of such biology where a spherical symmetry and more complex cell-to-cell interactions result in a more relevant biological model. Metabolism and the OCR is an important parameter, particularly considering the limited diffusion of O_2 and nutrients across the spheroid.

Such measurements can also be performed in microplate format whereby multiple spheroids are placed in a test well and measured as outlined above for differing cell lines, culture conditions and substrates. Figure 2.2 shows relative OCRs from spheroids of the human glioblastoma cell line U87MG and the human

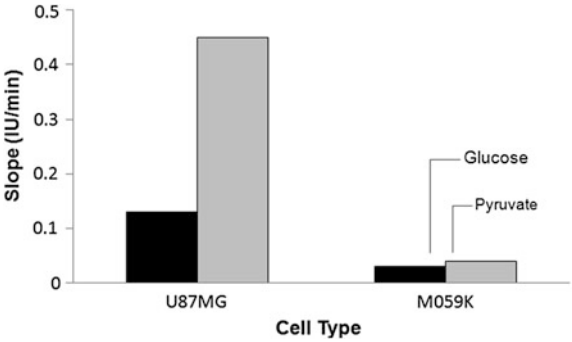

Fig. 2.2 Relative OCRs for U87MG, MO59 K spheroids pre-conditioned to glucose/pyruvate media for 4–6 h. Measurements conducted with spheroids from 1 mm average diameter at 3 spheroids per well of 96 well plate. (Data with permission from Michelle Potter, and Dr. Karl Morten, University of Oxford, U.K)

glioma cell line MO59 K, and the effect of glucose and pyruvate. U87MG spheroids are seen to be considerably more aerobic, and they show a significant increase in OCR when preconditioned in pyruvate compared to conventional glucose culture. A difficulty with the measurement of spheroids is the inherent variability that can exist in the amount of biomaterial in each replicate well due to variation in spheroid size. This can be addressed through the use of dedicated spheroid culture plates where the spheroids developed in a 'hanging drop' [34]. Using dedicated low volume plates, OCR of two or even one spheroid can be measured.

2.2.3 Analysis of Drug-Induced Mitochondrial Dysfunction by Parallel Measurement of OCR and Glycolytic Flux

While knowledge of cellular OCR provides direct information on OxPhos, an accompanying analysis of glycolysis, the other main ATP generating pathway in cells can also be valuable. This can be achieved by measuring the rate of extracellular acidification (ECA) of the media in which the cells grow. In an open system, the vast majority of this acidification is due to the production of lactic acid. The ECA can be followed using fluorescent pH-sensitive probes which, when spectrally compatible, facilitate true multiplexing where both probes are deployed together thereby reporting on both oxidative and glycolytic metabolism in the same test well. For example, the pH-sensitive probe pH-Xtra, which comprises a long decay narrow band emitting Eu(III)-chelate, can be multiplexed with Pt-porphyrin-based MitoXpress® ecO_2 probe (produced by Luxcel Biosciences, Ireland), to achieve simultaneous readout of O_2 and H^+ concentrations within the same sample with practically no cross-sensitivity [18]. pH-Xtra probe also changes its emission lifetime as a function of pH, so that both probes can be measured in RLD mode on standard TR-F readers.

It should be noted that, while such multiplexing is possible, from a data interpretation perspective, it is often simpler to conduct these measurements in parallel as the seal required for OCR measurements results in the trapping of Krebs

cycle derived CO_2 resulting in additional media acidification unrelated to glycolytic flux. A parallel measurement whereby OCR is measured in sealed wells and ECA is measured in unsealed wells is therefore preferable.

The compensatory mechanism outlined above, whereby cells can circumvent mitochondrial insult to maintain cellular ATP by increasing glycolytic flux, is particularly relevant to the investigation of drug-induced mitochondrial dysfunction. It can, however, be harnessed for screening whereby OCR is used as the primary indicator and ECA is used as a confirmatory parameter in both 96 and 384 well plate format. In such case, true mitochondria inhibitors will cause a decrease in O_2 consumption and an accompanying increase in ECA while general cell toxicity will cause a decrease in both parameters [18] as no compensation will be possible. Uncouplers would be expected to increase in both ECA and OCR. At the same time, it is important to be aware of the bell shaped dose response of ten associated with such uncouplers when interpreting such data (Fig. 2.1e). Figure 2.3 illustrates how this approach can be applied. A small library of drugs is screened at fixed concentration with data presented as to the strength of the response illicited. As expected, known inhibitors populate the top left quadrant indicating ETC inhibition and increased glycolytic flux while non-mitochondrial toxicants and those that inhibit upstream of glycolysis populate the bottom left quadrant. Uncouplers are expected to populate the top right quadrant indicating increased ETC and glycolytic flux. Compounds with no detectable effect at the test concentration populate the region around the origin. This approach is currently being expanded to include full dose response analysis and to examine the relationship between such metabolic screening and other available measurements of mitochondrial dysfunction.

2.2.4 Multi-Parametric Assessment of 'Cell Energy Budget'

The energy flux compensation illustrated in Sect. 2.2.3 has recently been developed further into the so-called 'Cell Energy Budget' (CEB) concept. CEB is particularly useful for the analysis of perturbed metabolism, mitochondrial and glycolytic disorders, which upon energy stress may lead to cellular malfunction and progression of various diseases [35–37].

OxPhos and glycolysis linked by the Krebs cycle serve as the main sources of ATP in eukaryotes, these pathways are mutually regulated in order to maintain optimal energy balance in the cell. The relative contribution of these pathways to cell bioenergetics varies broadly for different cell types and conditions. Other metabolic pathways also contribute to cell bioenergetics [38, 39], including β-oxidation of fatty acids, the pentose phosphate pathway and glutaminolysis, the latter is particularly important for cancer cell metabolism [40]. Normally, each of the main pathways has a considerable spare capacity outside the normal physiological range, thus allowing the cells to maintain stable ATP levels in stress conditions. However, metabolic abnormalities and mutations in genes linked directly or indirectly to OxPhos,

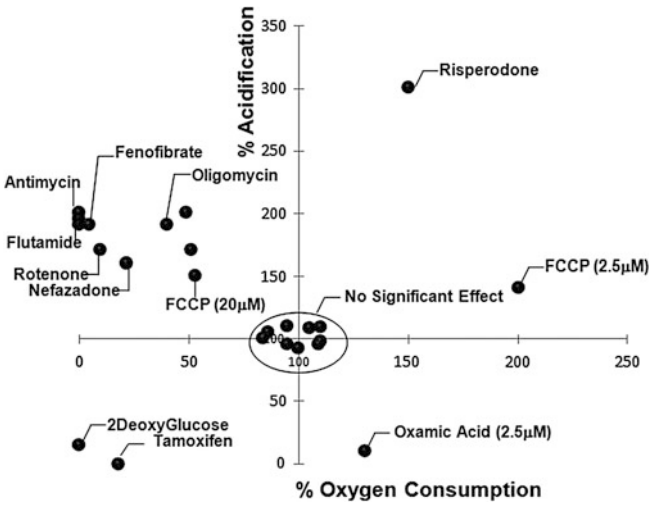

Fig. 2.3 Single concentration data analysis matrix assessing the effect of a panel of drugs on HepG2 cell metabolism including compounds of known mode of action

glycolysis, glutaminolysis or the Krebs cycle may alter their 'normal' contribution to ATP fluxes and reduce spare capacity [30, 40, 41]. For example in conditions of sustained excitation, shortage of nutrients or imbalance in energy-generating pathways the cells may be plunged into an energy crisis or become vulnerable to stress factors.

The main energy-generating pathways in eukaryotic cells and strategy for multi-parametric CEB assessment are shown schematically in Fig. 2.4. Their spare capacity can be probed pharmacologically or by limiting the corresponding substrates necessary for ATP production. Thus, in normal cells, total ATP levels remain unchanged for many hours when OxPhos is repressed by mitochondrial uncoupling [15] or when glycolysis is inhibited by substitution of glucose with galactose [26]. In such manner, spare capacity of different pathways and ability of the cells to utilise alternative ATP-producing pathway(s) can be quantified with appropriate bioassays.

In context of general cell metabolism, ATP fluxes through OxPhos and glycolysis, as well as the activity of the Krebs cycle, are more informative as direct bioenergetic parameters than cellular redox state, Ca^{2+} and NAD(P)H levels, mitochondrial membrane potential ($\Delta\Psi m$) and pH. Various technological platforms have been introduced recently for comparative quantitative analysis of the key metabolic parameters of the cells. The automated Extracellular Flux Analyser can accurately measure cellular OCR and ECA in a special microplate with built-in solid-state O_2 and pH sensors [43]; however, it is not able to differentiate between glycolytic and non-glycolytic contribution to the ECA. The more flexible platform based on the long decay emitting O_2 and pH sensitive probes overcomes this limitation [18, 44]. Using standard microtiter plates and TR-F plate reader detection, it can measure lactate in unsealed (L-ECA, CO_2 escapes from the

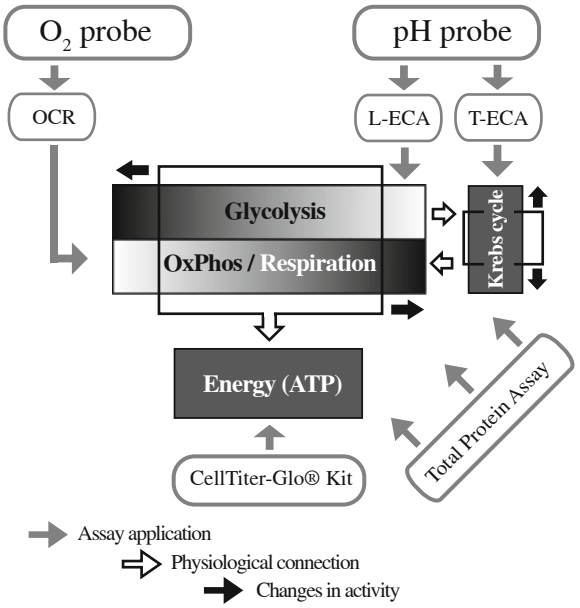

Fig. 2.4 Representation of the main energy-generating pathways in aerobic cells and strategy for CEB assessment showing the interrelationship of different pathways (*grey gradient color* and *white arrows*), ranges of physiological activity (*solid boxes*) and spare capacity (*dark arrows*). The bioassays used in quantitative CEB analysis are shown in grey boxes. Adapted from [42]

medium) and lactate plus CO_2 in sealed samples (total, T-ECA), thus discriminating between the glycolytic and non-glycolytic ECA components. Together with the measurement of OCR and total ATP levels, this CEB platform provided a detailed assessment of the contribution of each of the three main energy-generating pathways [42]. Notably, the main producer of CO_2 in the cell is the Krebs cycle, while the pentose phosphate pathway and pyruvate/malate cycle also produce CO_2 [45, 46].

To assess CEB with a minimal set of experiments, measurement of the cellular OCR, T-ECA, L-ECA and ATP values is conducted under both resting conditions and upon double treatment with FCCP/oligomycin. Inhibition of OxPhos by oligomycin can be used to probe mitochondrial respiration uncoupled from ATP production; however, oligomycin also increases proton motive force across the mitochondrial inner membrane and elevates the rate of proton leak, thus making the results difficult to interpret. In contrast, oligomycin/FCCP treatment strongly activates the OCR due to uncoupling and prevents the production and hydrolysis of ATP by Complex V. To compensate for decreased flux of mitochondrial ATP, the cells are forced to increase their glycolytic ATP production.

Individual metabolic assays and organisation of the CEB assessment are described in Table 2.1. The OCR and T-ECA are measured in sealed samples covered with oil to prevent back diffusion of ambient O_2 and escape of CO_2. They both can be measured in one kinetic assay on the first plate, and values expressed as relative changes of primary luminescent parameters over time, i.e. intensity or lifetime slopes. Similarly, the L-ECA and total ATP are both measured in unsealed samples exposed to ambient air. These assays can be performed sequentially on the

second plate: after the completion of the kinetic L-ECA assay, total ATP is measured by cell lysis and end-point measurement of bioluminescent signals.

To reduce experimental error associated with different batches of cells and plates, resting and FCCP/oligomycin uncoupled cells are recommended to measure on the same plate. For accurate cross-comparison of different cell types, measured raw values of bioenergetic parameters should be normalised for different biomass content in corresponding samples, which can be determined in a separate experiment by measuring total protein concentration. In this manner, up to 96 or even 384 samples can be analysed in parallel on the same plate, producing comprehensive sets of data for different conditions, treatments and cell types. Necessary repeats, blanks and positive controls (reference or untreated cells) are also incorporated, as required.

The CEB approach was successfully applied to analyse the role of fumarate hydratase enzyme (FH) in cell energy production. Inactivating mutations of the gene encoding FH are known to cause a number of human cancers including hereditary leiomyomatosis and renal cell cancer (HLRCC) [47]. FH is localised predominantly in the mitochondria and at lower levels in the cytosol [48], and catalyses conversion of fumarate to malate [49]. This reaction is a critically important step of the Krebs cycle and determines the respiratory activity of the cell. FH deficiency in mouse embryonic fibroblasts (MEFs) strongly affects mitochondrial function leading to reduced mitochondrial respiration and elevated glycolysis [41].

This was further investigated by a comparative CEB assessment of the wild type (WT, $Fh1^{+/+}$) and $Fh1^{-/-}$ knockout (KO) MEFs. The KO cells were significantly smaller, so they were seeded at higher numbers than WT cells and for proper comparison the results were normalised for total protein content. OCR measurements with resting cells revealed a dramatic difference in OCR between the WT and KO cells (Fig. 2.5a). Upon uncoupling the OCR in WT cells increased by approximately twofold, while in KO cells it did not change indicating their low spare respiratory capacity [42]. ATP levels in KO were also lower than in WT cells (Fig. 2.5b), but upon uncoupling they stayed unchanged in both cell lines. As shown by L-ECA data, glycolysis of resting KO cells was increased $\sim$2-fold compared to the WT (Fig. 2.5c): 1.25 pH unit/min/10^6 cells. Upon uncoupling, L-ECA in WT cells increased $\sim$2-fold (shown by the arrow) to compensate for the loss of OxPhos flux, whereas in KO cells L-ECA remained unchanged. This is because most of the ATP in KO cells was already produced through glycolysis. The difference between L-ECA and T-ECA in KO cells was small due to a smaller contribution of the Krebs cycle in CO_2 production. The large decrease in OCR/L-ECA ratio for KO cells reflects the shift in CEB toward glycolytic energy production (Fig. 2.5d). This study demonstrates practical use of quantitative CEB assessment and O_2 monitoring as one of its key parameters.

Table 2.1 Proposed layout and description of the panel of metabolic assays used for CEB assessment. Multiplexable assays are colour coded and assigned plate number

Assay No	Description	Format	Samples	Measured parameters	Plate No.
1.	OxPhos activity Kinetic assay with MitoXpress® Probe (340/650 nm)	Sealed samples in 96/384 WP	Resting and uncoupled cells Panels of cells, different conditions and treatments	Respiration/OCR: R_b and R_{max}	1
2.	Glycolytic Flux Kinetic assay with pH-Xtra Probe (340/615 nm)	Unsealed samples in 96/384 WP	Resting and uncoupled cells Panels of cells, different conditions and treatments	L-ECA G_b and G_{max}	2
3.	Krebs Cycle Activity Kinetic assay with pH-Xtra Probe (340/615 nm)	Sealed samples in 96/384 WP	Resting and uncoupled cells Panels of cells, different conditions and treatments	T-ECA vs L-ECA K_b and K_{max}	1
4.	ATP Assay, CellTiter-Glo® Kit (Promega)—BL measurement after cell lysis (end point, after assay 2)	Unsealed samples in 96/384 WP	Resting and uncoupled cells Panels of cells, different conditions and treatments	Total cellular ATP levels	2
5.	BCA™ Protein Assay—total protein measurement after cell lysis with convenient buffer containing detergent (end-point)	Unsealed samples in 96/384 WP	Different cells, long-term culture or treatments	Relative biomass content	3

Note R_b, R_{max}, G_b, G_{max}, K_b and K_{max}—basal and maximal capacity of respiration (R), glycolysis (G) and Krebs cycle (K), respectively. Spare capacity is the difference of the two values

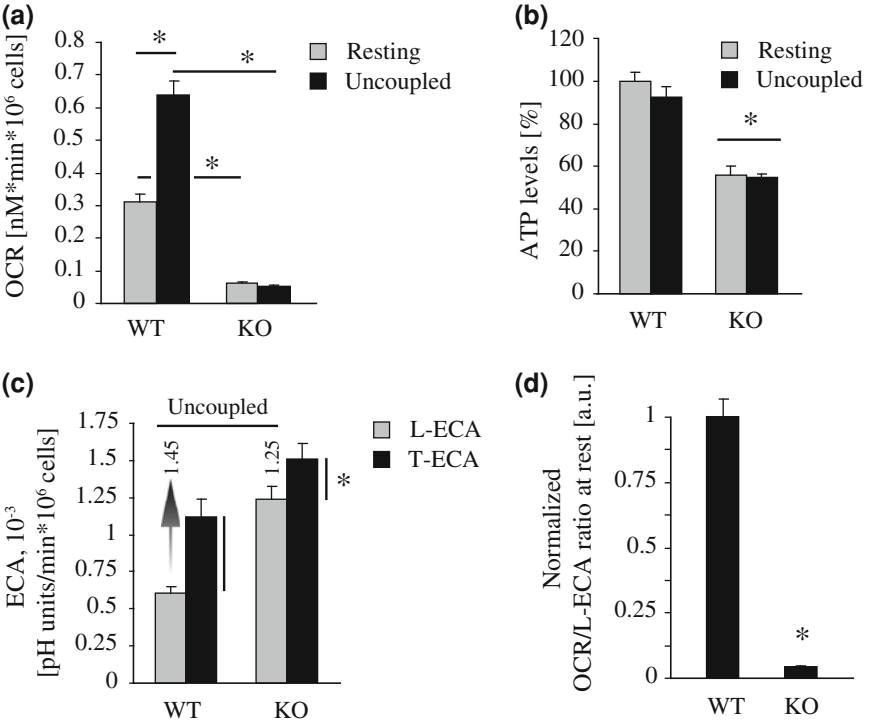

Fig. 2.5 Glycolytic shift in CEB associated with FH deficiency in MEF cells. **a** OCRs for the WT and KO MEF cells at rest and upon uncoupling with 1 μM FCCP/10 μM oligomycin. **b** Total ATP levels. **c** L-ECA and T-ECA for the resting cells. Arrows show their increase upon uncoupling. **d** OCR/L-ECA ration is dramatically reduced in KO cells. Asterisks indicate significant differences. Transformed FH cells were kindly provided by Julie Adam and Patrick Pollard, University of Oxford, UK

2.2.5 Monitoring of Oxygenation and Cell Respiration in Microfluidic Biochips

A number of microfluidic chips and microchamber devices developed for biological applications including cell-based assays are now produced commercially. Such devices are often characterised by restricted permeation of atmospheric O_2 through biochip material, and limited diffusion of dissolved O_2 through their long and narrow-bore flow channels. When respiring cells and other biological samples are placed in such devices, control of oxygenation (and other relevant parameters such as pH, CO_2) becomes very important. Unfortunately, such control systems are not always considered and implemented by either the developers or end-users of such biochips.

Among the critical factors that determine the behaviour of the cells in biochip systems are cell density, O_2 availability, cell stress during the seeding and

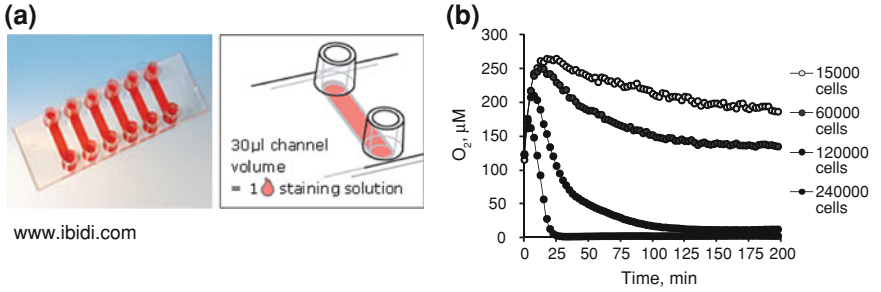

Fig. 2.6 Monitoring of cell deoxygenation with μ-slide $VI^{0.4}$ microchambers (Ibidi). **a** - images of the device. **b** - time profiles of oxygenation of adherent non-differentiated PC12 cells seeded at indicated numbers (per chamber, in 30 µL volume) and measured with the help of extracellular probe MitoXpress® on Victor2 reader

attachment (stopped flow conditions), changes in cell respiration rate and prolonged measurements under static or limited O_2 supply conditions. These factors may cause rapid depletion of dissolved O_2 within the microchamber leading to hypoxic/anoxic shock, altered function or cell death. In this regard, O_2 sensing probes and phosphorescence quenching techniques provide simple tools for non-invasive, real-time monitoring of oxygenation conditions within biochips with cells and tissue samples. Such systems are more flexible and versatile than fibre-optic O_2 micro-sensors or solid-state coatings embedded in the biochips.

With an appropriate set-up, ecO_2 probes can be used in conjunction with commercial biochips to conduct simple O_2 assays and OCR measurements, an approach which is particularly useful when measuring with microscopic samples containing delicate cells preparations. They can also be used to optimise assay conditions and conduct the O_2 assays in a convenient and reproducible manner on commercial fluorescent readers. For example, Ibidi μ-slide microchambers (Fig. 2.6a and [50]) have been designed for optical microscopy imaging of both suspension and adherent cells that can be loaded manually with a micropipette. Such biochips with surfaces treated for cell attachment can also be used in prolonged experiments with adherent cells.

Thus, using 6-channel Ibidi μ-slides, oxygenation conditions and cell behaviour under resting or re-perfusion conditions, were analysed using the MitoXpress® probe and measurements on a standard TR-F reader equipped with an adaptor holder for microscopy slides. The analysis of non-differentiated PC12 cells seeded at different densities inside the biochip, revealed a rapid deoxygenation of the chamber (Fig. 2.6b). Thus, at 60,000 cells per chamber (in 30 µL of medium) a level of 150 µM O_2 was reached after 2–3 h of monitoring. This is noteworthy as such densities are commonly used for DNA transfection while at higher cell densities anoxic conditions were quickly established. These data show that under the static conditions such as those used during cell attachment, cell seeded in air-saturated medium ($\sim$200 µM) can become deeply deoxygenated and experience hypoxia-induced physiological responses. From Fig. 2.6b, it is also evident that

the rate of diffusion of ambient air O_2 through Ibidi μ-slide microchamber material is significant. At densities of 15,000 and 60,000 cells per chamber steady-state conditions were established after 2–3 h whereby cellular O_2 consumption is balanced by back diffusion. Therefore by changing the microchamber material, cell density, atmospheric pO_2 or flow conditions one can modulate cell oxygenation. These results also show that this measurement platform can be applied for rapid OCR measurements. Respiration profiles and such measurements tend to be faster and more sensitive than standard 96-well microplate measurements while also allowing repeat treatments by flushing the microchambers with fresh air-saturated medium, or drug.

2.2.6 Analysis of Microbial Cell Cultures

While OCR measurement is widely applied to the analysis of mammalian cells and organelles, there are also a wide variety of microbiological applications, both prokaryotic and eukaryotic. These are often based on rapid cellular growth and therefore require a slightly different approach: at low cell numbers the level of depletion of dissolved O_2 is not sufficient out strip back diffusion resulting in no signal change since the sample remains oxygenated. However, as bacteria replicate the level of O_2 consumption increases until a critical point is reached and the sample begins to deoxygenate rapidly causing a robust increase in the signal from ecO$_2$ probe. Figure 2.7a illustrates this type of data output whereby increasing *E.coli* seeing concentration results in earlier spike in probe signal. Such curves are amenable to an 'onset-time' data analysis approach where the time taken to reach a defined signal threshold is the output metric. Figure 2.7b illustrates the relationship between seeding concentration and such a metric, with nice linear plots in semi-logarithmic scale. Again, phosphorescence lifetime is a preferred readout parameter as it is more stable than intensity signals.

The simplicity and robust nature of the oxygenation-based growth profiles generated using phosphorescent O_2 probes has led to it being adapted for a variety of application. Examples include the enumeration of bacterial load in complex samples such as food homogenates, environmental and wastewater samples using microtiter plates (96 and 384-well), thereby avoiding the need for standard aerobic plate counting and multiple dilutions [20]. Figure 2.7c illustrates the data output of such analysis of ground beef with higher bacterial load reflected by an earlier onset-time. These onset times can then be converted to bacterial load values, using a pre-determined calibration. Figure 2.7d shows this conversion with load presented in CFU/mg and a 'flag' calculated based on defined acceptance criteria.

This measurements approach can also be used for the optimisation of culture conditions, for screening applications and determination of drug resistance. A dose response analysis is presented in Fig. 2.8 where *S.aureus* seeded at $\sim 1 \times 10^7$ cells/ml are exposed to increasing concentrations of antibiotic and O_2 depletion is measured kinetically. The respiration profile for all test wells is presented and, as

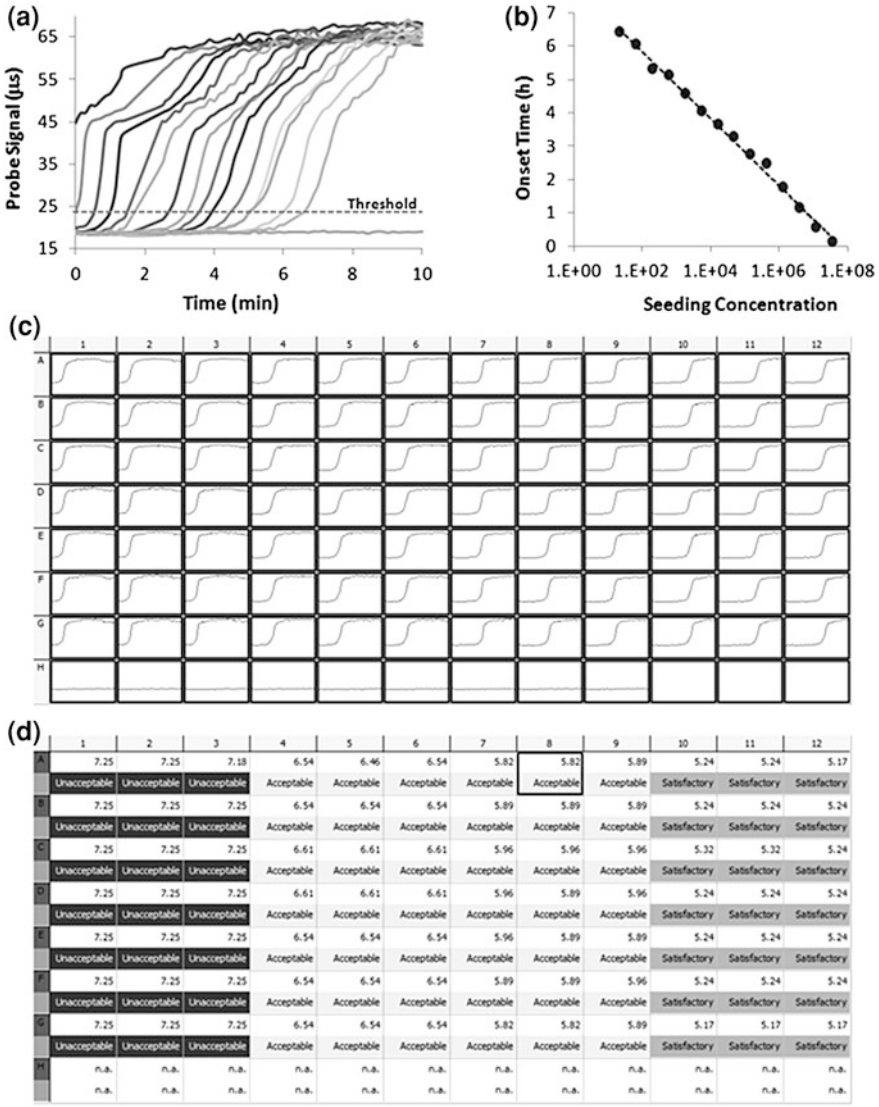

	1	2	3	4	5	6	7	8	9	10	11	12
A	7.25	7.25	7.18	6.54	6.46	6.54	5.82	5.82	5.89	5.24	5.24	5.17
	Unacceptable	Unacceptable	Unacceptable	Acceptable	Acceptable	Acceptable	Acceptable	Acceptable	Acceptable	Satisfactory	Satisfactory	Satisfactory
B	7.25	7.25	7.25	6.54	6.54	6.54	5.89	5.89	5.89	5.24	5.24	5.24
	Unacceptable	Unacceptable	Unacceptable	Acceptable	Acceptable	Acceptable	Acceptable	Acceptable	Acceptable	Satisfactory	Satisfactory	Satisfactory
C	7.25	7.25	7.25	6.61	6.61	6.61	5.96	5.96	5.96	5.32	5.32	5.24
	Unacceptable	Unacceptable	Unacceptable	Acceptable	Acceptable	Acceptable	Acceptable	Acceptable	Acceptable	Satisfactory	Satisfactory	Satisfactory
D	7.25	7.25	7.25	6.61	6.61	6.61	5.96	5.89	5.96	5.24	5.24	5.24
	Unacceptable	Unacceptable	Unacceptable	Acceptable	Acceptable	Acceptable	Acceptable	Acceptable	Acceptable	Satisfactory	Satisfactory	Satisfactory
E	7.25	7.25	7.25	6.54	6.54	6.54	5.96	5.89	5.89	5.24	5.24	5.24
	Unacceptable	Unacceptable	Unacceptable	Acceptable	Acceptable	Acceptable	Acceptable	Acceptable	Acceptable	Satisfactory	Satisfactory	Satisfactory
F	7.25	7.25	7.25	6.54	6.54	6.54	5.89	5.89	5.96	5.24	5.24	5.24
	Unacceptable	Unacceptable	Unacceptable	Acceptable	Acceptable	Acceptable	Acceptable	Acceptable	Acceptable	Satisfactory	Satisfactory	Satisfactory
G	7.25	7.25	7.25	6.54	6.54	6.54	5.82	5.82	5.89	5.17	5.17	5.17
	Unacceptable	Unacceptable	Unacceptable	Acceptable	Acceptable	Acceptable	Acceptable	Acceptable	Acceptable	Satisfactory	Satisfactory	Satisfactory
H	n.a.	n.a.	n.a.	n.a.	n.a.	n.a.	n.a.	n.a.	n.a.	n.a.	n.a.	n.a.
	n.a.	n.a.	n.a.	n.a.	n.a.	n.a.	n.a.	n.a.	n.a.	n.a.	n.a.	n.a.

Fig. 2.7 Assessing bacterial respiration showing O_2-based E.coli growth curves (**a**), the relationship between seeding concentration and onset-time (**b**), the data output from bacterial load assessment showing the profiles measured in each well (**c**) and the calculated bacterial load in CFU/mg and a 'flag' based on this load (**d**)

above, the time at which probe signal increases indicates the degree to which growth has been inhibited with flat lines indicating complete inhibition. Onset times can, subsequently, be calculated for the generation of IC_{50} and MIC values.

Such an approach can also be applied to the analysis of yeast metabolism where a longer doubling time means that high cell numbers and short measurement times

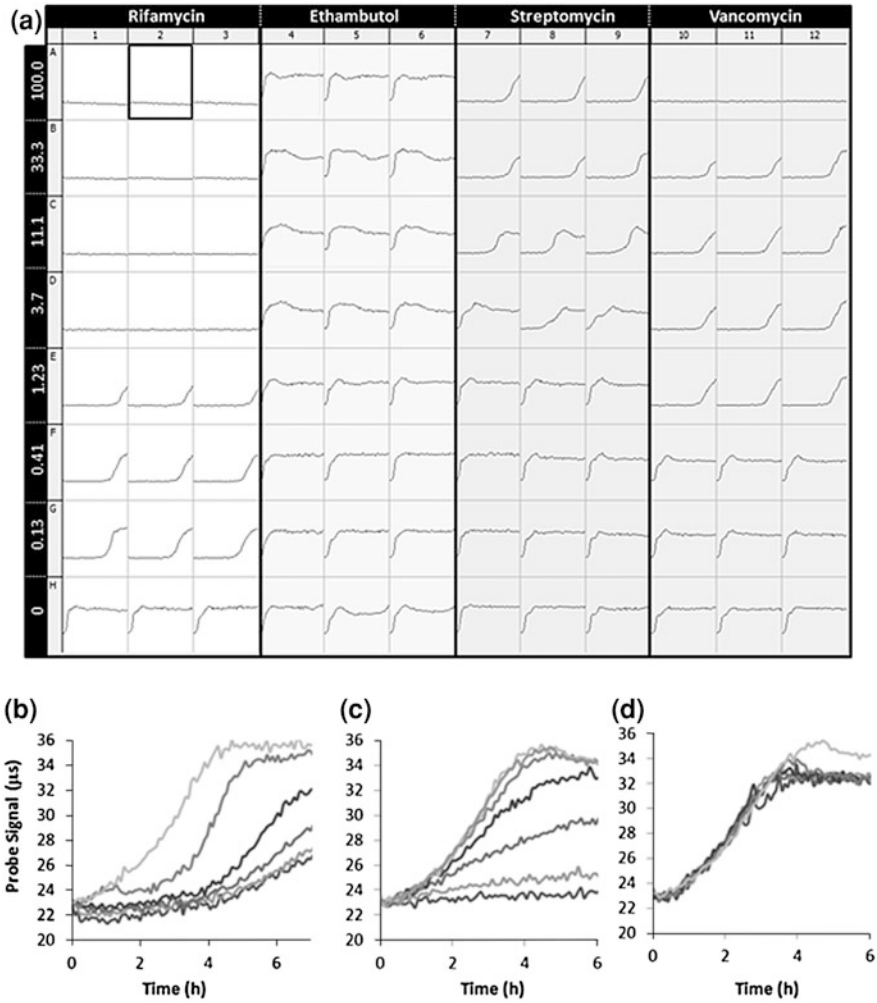

Fig. 2.8 **a** *S.aureus* seeded at $\sim 1 \times 10^7$ cells/ml in EB broth, exposed to increasing concentrations of the indicated antibiotic and measured kinetically at 37 °C. The drug tested is indicated above the relevant wells with the treatment concentration to the left. **b–d** O_2 consumption profiles from *C.albicans* ($\sim 3 \times 10^5$ cells/ml) treated with increasing concentrations Ant A (from 30 µM), Amphotericin (from 16 µg/ml) and Fluconazone (from 65 µg/ml) in RPMI medium

allows the assessment of immediate effects on cell metabolism while using lower cell numbers and extended measurement times facilitates analysis of effect on cell growth and metabolism. Figure 2.8a presents a series of *C.albicans* dose responses. The ETC inhibitor Ant A (Fig. 2.8b) and the polyene antifungal Amphotericin B (Fig. 2.8c) cause an immediate and dose-dependent decreases in O_2 consumption while the triazole antifungal Fluconazole (Fig. 2.8d) caused no appreciable decrease in OCR. These observations correlate with mode of drug action and

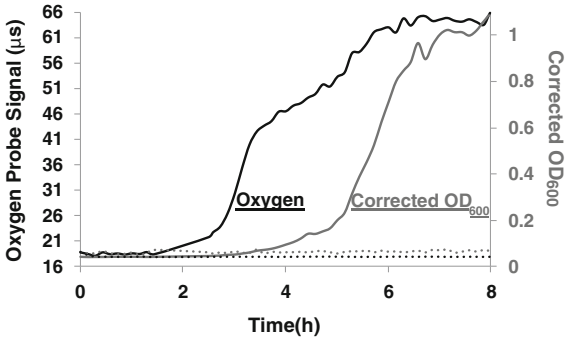

Fig. 2.9 Comparison between O_2 and OD_{600} based growth curves from an *E.coli* culture seeded at 1.3×10^5 cells/ml

demonstrate how such measurements can be used to assess the specific metabolic effects of compound treatment.

Where applicable, additional levels of detail can be gleaned from the whole shape of the respiration profile, which can point to the type of microorganism(s) present in the sample. Furthermore, a multiplexed luminescence-based O_2 and absorbance-based measurement of bacterial cultures (turbidimetry, OD_{600}) can be conducted whereby both parameters are measured in the same test well. This allows an assessment of the relationship between O_2 dependent metabolism and increases in biomass. Figure 2.9 presents such a multiplexed measurement whereby *E.coli* seeded at $\sim 1 \times 10^5$ cells/ml are monitored with O_2 depletion occurring significantly earlier than measurable increased in OD_{600}. Such measurement can also be used to assess the contribution of aerobic metabolism to the energy required for growth, but such a multiplexed approach can only be applied under certain conditions as stable OD_{600} growth curves can sometimes be difficult to generate particularly in opaque or coloured growth media. O_2 measurements are much more flexible and robust in this regard, particularly when using the lifetime-based measurement modality and data analysis approach.

2.2.7 Respiration of Small Organisms and Model Animals

While the majority of applications of optical O_2 micro-respirometry and OCR measurement are cell-based, the method has also been adapted for the monitoring of small aquatic organisms including *Daphnia magna*, *Artemia salina*, copepod *Tigriopus*, zebrafish *Danio rerio* [3, 4]. These model organisms can be used to perform rapid, high-throughput biological testing of potentially hazardous chemicals and environmental samples, as well as basic biological and physiological studies. In such assays, test organisms are exposed to a particular condition (development stage, environment, potential toxicant or stress) and then allowed to respire in a sealed compartment in the presence of an ecO_2 probe. The resultant O_2 depletion causes an increase in probe phosphorescence over time, reflecting the metabolic activity of the organism. The appropriate measurement platform is

selected from the available options (Chap. 1, Fig. 1.5), based on the respiration activity and size of test organism, and specific application requirements.

For example, this method was applied to the measurement of individual *Daphnia magna* after 24 and 48 h toxicant exposures, using low-volume sealable 96-well plates and MitoXpress® probe [51]. The respirometric measurements performed with reference toxicants including $K_2Cr_2O_7$, sodium lauryl sulphate and heavy metals, showed good agreement with the established *Daphnia* test based on mortality assessment while the ability to analyse sub-lethal effects and complex samples such as industrial effluents, facilitates the generation of dose–response relationships and EC_{50} values. Representative profiles of *Daphnia magna* respiration are shown in Fig. 2.10. Zebrafish *Danio rerio*, another useful model for genetic manipulation, toxicological studies and environmental monitoring, was also applied for toxicological assessment by measuring respiration of individual embryos (48 h after hatching) [52].

Organisms such as *Caenorhabditis elegans* have also been measured. This is an interesting model organism as it is a non-parasitic, multicellular metazoan with a 3-day lifecycle and is commonly used in developmental biology, behavior, anatomy and genetics studies offering relevant endpoints such as mortality, life span, behavior/movement, feeding, growth and reproduction. This invertebrate organism easily maintained under laboratory conditions is an attractive model for toxicology studies as it is sensitive to a wide range of toxicants, including heavy metals, organic phosphates and pesticides. Such studies have established *C. elegans* as a powerful model for rapid testing of the toxicity of soil and water samples as well as pharmaceutical compounds [53].

Another system for toxicological assessment uses panels of test organisms which include prokaryotic (*E. coli*, *V. fischeri*) and eukaryotic (Jurkat) cells, invertebrate (*Artemia salina*) and vertebrate (*Danio rerio*) organisms. Convenient assay set-up allows parallel assessment of up to 96 samples or data points in $\sim$2 h, and the generation of dose and time-dependent responses in both standard and low-volume 96-well plates. The methodology was demonstrated with discrete chemical classes including heavy metal ions, PAHs and pesticides, chemical mixtures and complex environmental samples such as wastewater from a WWTP. Compared to the single organism testing, this system provides more detailed information and allows profiling of different toxicants on the basis of the pattern of their response. Representative results and patterns of toxicity are shown in Fig. 2.11. The panel of organisms can also be modified or extended.

Such toxicological screening systems provide high sensitivity, sample throughput and information content, flexibility and general robustness. They allows ranking and profiling of samples and compare favourably with the established methods such as MicroTox®, Daphnia Test and mortality tests with animal models. They are well suited for large-scale monitoring programmes such as the US Clean Water Act, EU Water Framework Directive and EU REACH (Registration, Evaluation and Assessment of Chemicals) programme.

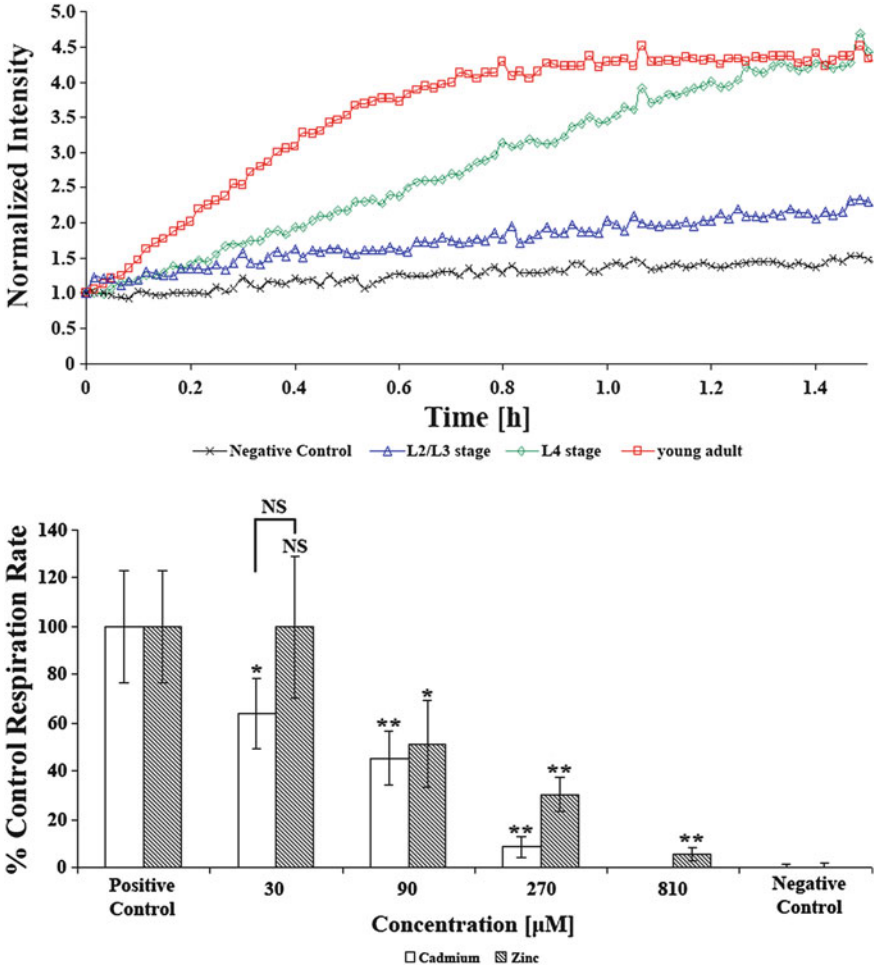

Fig. 2.10 Respiration profiles of individual *C. elegans* at different age (*top*) and the effects of their 24 h exposure to different concentration of heavy metal ions (Zn and Cd, as indicated). Measured in low-volume sealable 96-well microplates at room temperature. Reproduced from [53], with permission of Wiley

2.2.8 Enzymatic Assays

O_2-consuming enzymes play an important role in many biochemical pathways. They also have diagnostic value and screening potential, and therefore have become the focus of attention both as drug targets and as players in drug metabolism. Common examples include the monoamine oxidase (MAO), cytochrome P450 (CYP450) and cyclooxygenase (COX) families, glucose oxidase and

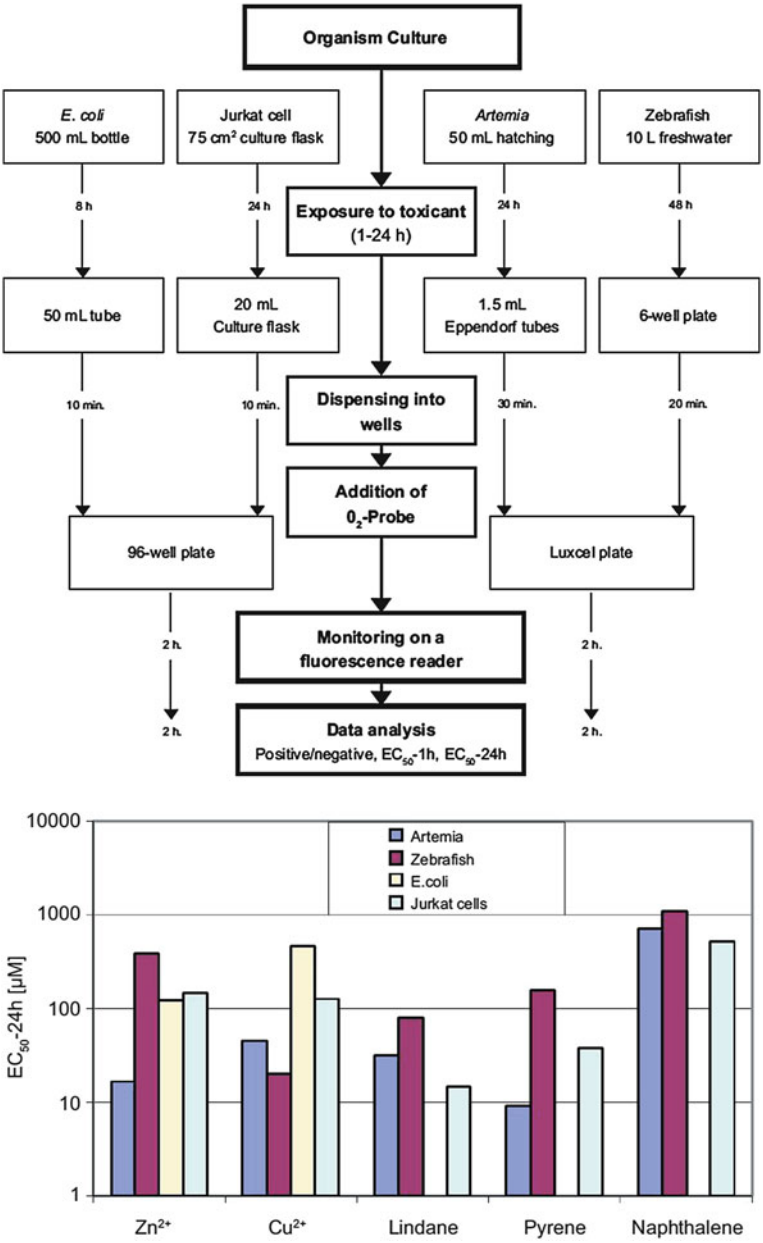

Fig. 2.11 Scheme of toxicological assessment of samples using panels of test organisms and O_2 respirometry (*top*) and representative results (*bottom*). Reproduced from [52] with permission of Wiley

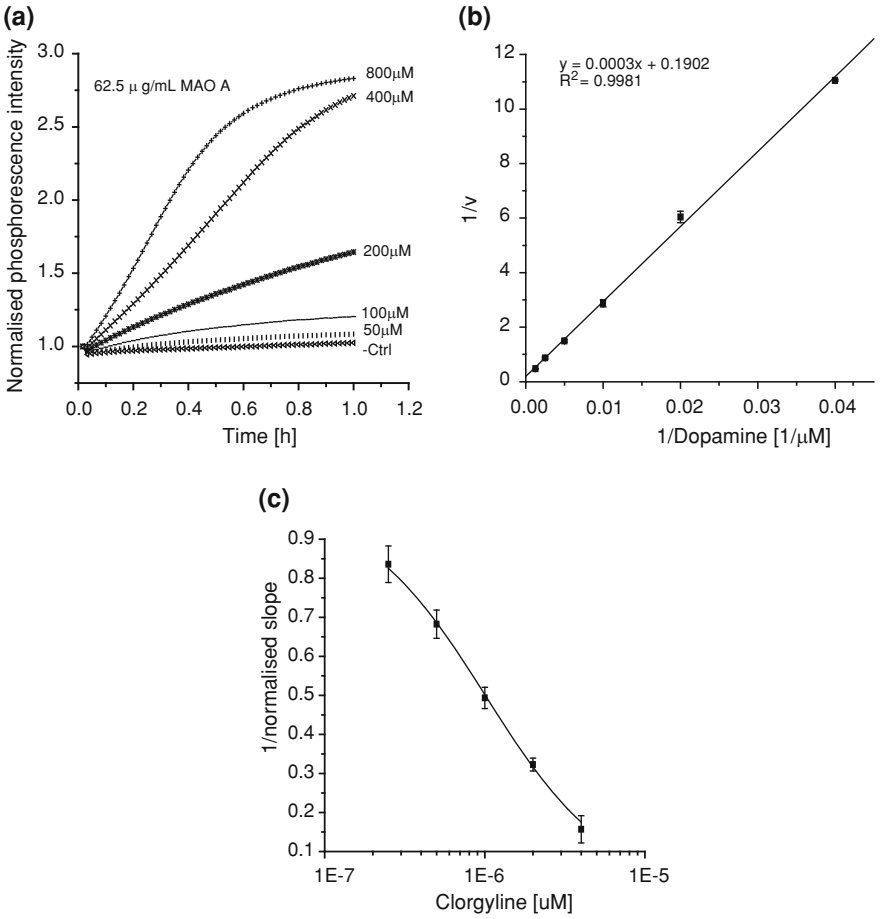

Fig. 2.12 **a** Normalised intensity profiles for 62.5 μg/ml MAO-A enzyme at different concentrations of dopamine; **b** The relationship between reciprocal reaction rate (*slope*) and substrate concentration (derived from A) is linear. **c** Inhibition of MAO-A activity (0.125 mg/ml and 0.4 mM of dopamine) by clorgyline: inversed normalised slopes versus inhibitor concentration. Measured with 5 μM MitoXpress probe at 37 °C, in three replicates for each point ($n = 3$, error bars are shown). Adapted from [6] with permission of Analytical Biochemistry and Elsevier

lactate oxidase. Again the optical O_2 sensing technique provides convenient means for monitoring of activity and inhibition of a particular enzyme quantification of their substrates and inhibitors, control of production and characterisation of recombinant enzymes (oxidases). Similar to the mitochondria and cell-based applications described above, such enzymatic assays can be conducted in a convenient 96/384-well plate format using simple mix-and-measure procedure and measurement on a fluorescent plate reader of samples sealed under oil, similar to the assays with isolated mitochondria (see Sect. 2.2.1).

The capillary-based LightCycler system was also shown to be efficient in such applications, providing assay miniaturisation, better sensitivity and reproducibility compared to microplate assays. Using the phosphorescence-based molecular and nanoparticle probes solid-state sensor coatings, this platform was demonstrated with the analysis of important oxygenases (MAO, COX and CYP450 families) and their specific inhibitors [6]. Representative O_2 consumption profiles and their transformation into calibration curves for the quantification of the substrate and inhibitors are shown in Fig. 2.12. Sensitive detection of cholinesterase inhibitors in a coupled enzymatic system of acetylcholinesterase—choline oxidase was also demonstrated using optical O_2 detection and the LightCycler® system [54].

Besides the above examples and case studies, a number of other specimens, including plant mitochondria, seeds (analysis of germination), different types of microbial and mammalian cells, have been analysed and used in various mechanistic studies on cell metabolism, mitochondrial function and signalling, in conjunction with the phosphorescent ecO_2 probes and plate reader analysis. All these demonstrate the versatility of this sensor chemistry and measurement methodology and the large number of analytical tasks they can perform.

2.3 Bioassays Performed with icO_2 Probes

It is known that oxygenation of live tissue is significantly lower than dissolved O_2 concentration in air-saturated solution ($\sim$200 μM or 158 mmHg at normal atmospheric pressure, 20.9 % O_2, 37 °C). Thus, measured in arteries, brain and retina O_2 levels were found to be $\sim$97.5, 1–40 and 2–5 mmHg, respectively [55, 56]. Upon pathological conditions or disease states O_2 levels in the cells may further decrease, leading to energy stress, activation of adaptive responses and, ultimately, cell survival or death. Therefore, it is difficult to overestimate the importance of precise monitoring of the cell oxygenation as a key metabolic parameter, which informs on cell functioning and helps to predict cell fate. Pt-porphyrin-based icO_2 probes are well suited to quantitative real-time monitoring of O_2 in various biological samples, from cell populations to sophisticated 3D specimens and O_2 mapping in complex heterogeneous samples (as outlined in Chap. 3).

2.3.1 Relationship Between Respiratory Activity, Sample Parameters and Oxygenation

Mathematical modelling facilitates a better understanding of the various biophysical processes taking place in biological samples [57, 58] and helps with the comparison of experimental data and theoretical models. A limitation, however, is that available experimental techniques often have limited capacity to explicitly

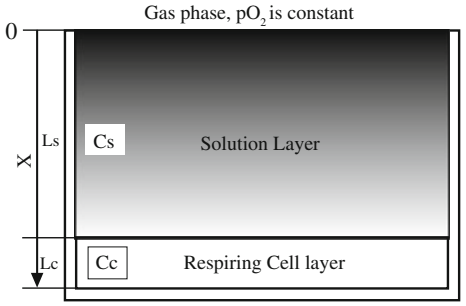

Fig. 2.13 Physical model of a biological sample containing a monolayer of respiring cells in growth medium exposed to atmospheric O_2

confirm the models in question. New techniques are therefore required to address this gap and the O_2 measurements described here contribute to this. Since respiration of cells and tissues has a complex dependence on O_2 concentration, a precise analytical description of O_2 dynamics in different parts of a 3D sample is difficult. However, for simpler models often used in in vitro studies, such as individual cells suspensions (spherical model), monolayers of adherent cells (2D) or spheroids and scaffolds (3D), mathematical description of localized O_2 gradients and O_2 mapping, can be realised in relatively simple mathematical terms [59].

Thus, for a simple planar model of adherent respiring cells maintained in a vessel with headspace under static culturing conditions (e.g. samples in microplate wells—Fig. 2.13), O_2 concentration in the solution layer (Cs) and within the cell layer (Cc) can be described by simple mathematical equations. Using a number of valid assumptions, one can work out that the profiles of Cs and Cc within the sample obey the linear and quadratic functions of the distance from the headspace which serves as an O_2 reservoir, and the thickness of the *Ls* and *Lc* layers [59]:

$$Cs = C_0 - \frac{Lc}{Ds}k(X + Ls) \tag{2.1}$$

$$Cc = \frac{k}{2Dc}X^2 - k\frac{Lc}{Dc}X + H\left(C_0 - \frac{LcLs}{Ds}k\right) \tag{2.2}$$

In these equations, C_0 is O_2 concentration at the gas/solution interface ($X = 0$) at given O_2 and temperature; *Dc* and *Ds*–O_2 diffusion coefficients in solution and cell layers; H–O_2 partition coefficient at cells/solution interface ($Cc|_{X=Ls} = HCs|_{X=Ls}$); X—distance from the interface and *k*—specific respiratory activity of the cell layer. The model suggests that actively respiring cells can generate local O_2 gradient in the sample, and this can be assessed by means of:

An ecO_2 probe which informs on the *Cs* in the medium. When measured on a plate reader through the sample, it produces *Cs* values averaged across the whole depth of medium layer above the cells;

An icO_2 probe which informs on *Cc* within cell monolayer. Due to the small thickness of this layer (~ 10 μm), the O_2 gradient across it is deemed very small so that oxygenation of the cells is relatively uniform and corresponds to the measured *Cc* value. Hence, icO_2 probes enable accurate measurement of oxygenation of cell

layers and through this parameter monitoring of sustained or transient changes in respiration, associated with cell metabolic activity, the levels of atmospheric pO_2 or drug action.

2.3.2 Cell Loading and Optical Measurements with icO_2 Probes

For probes developed specifically for intracellular use, loading usually involves addition to complete growth medium at concentrations optimised in separate experiments or provided by the vendor, and incubating the cells under standard culturing conditions for several hours (3–16 h or shorter) in a CO_2 incubator at 37 °C. After washing and change to fresh medium, the plate with cells is ready for measurements and treatments.

Although cell-permeable probes enable the measurement of icO_2 in a simple mix-and-measure format, a number of factors have to be considered. For reliable and accurate lifetime-based O_2 sensing, the phosphorescent signals produced by samples of loaded cells should be enough high to ensure signal-to-blank ratio (S:B) of at least 10. The intensity signals, in turn, are determined by the following parameters:

(1) Probe loading concentration and incubation time. With the example of NanO2 probe typical dependences can be seen in Fig. 2.14, which look almost linear without sign of saturation. This probe even when used at low very doses (2–5 μg/ml) produces very high signals in different cell types, which may exceed 10^5–10^6 cps (counts/photons per second) and even cause detector saturation at high concentrations. However, for other icO_2 probes loading efficiency and kinetics may be very different and acceptable levels of signals for reliable sensing of icO_2 may not so easy to reach. For the high-sensitivity TR-F reader Victor^4 in our lab the acceptable signal threshold was set at 30,000 cps and blanks were typically <1,000 cps. But again for another instrument the threshold and blanks may be quite different due to different instrument performance or intensity scale used (luminescence spectroscopy operates with arbitrary intensity units).
(2) The density or number of cells in the sample. Generally, the more cells in the sample the higher the phosphorescent signals after loading. At very low cell numbers the signals can drop below the acceptable threshold which will result in increased error in lifetime and O_2 determination. At low cell density local O_2 gradients vanish due to low levels of respiration (see below), while very high cell numbers can cause complete deoxygenation, hypoxic shock and death of the cells.
(3) Atmospheric O_2 levels and oxygenation of the medium and cell monolayer. Given that phosphorescence intensity signals are inversely related to O_2 concentration (see Eq. 1.1) and that the O_2 sensing method provides best performance and resolution at zero O_2 [12], measurements under low O_2

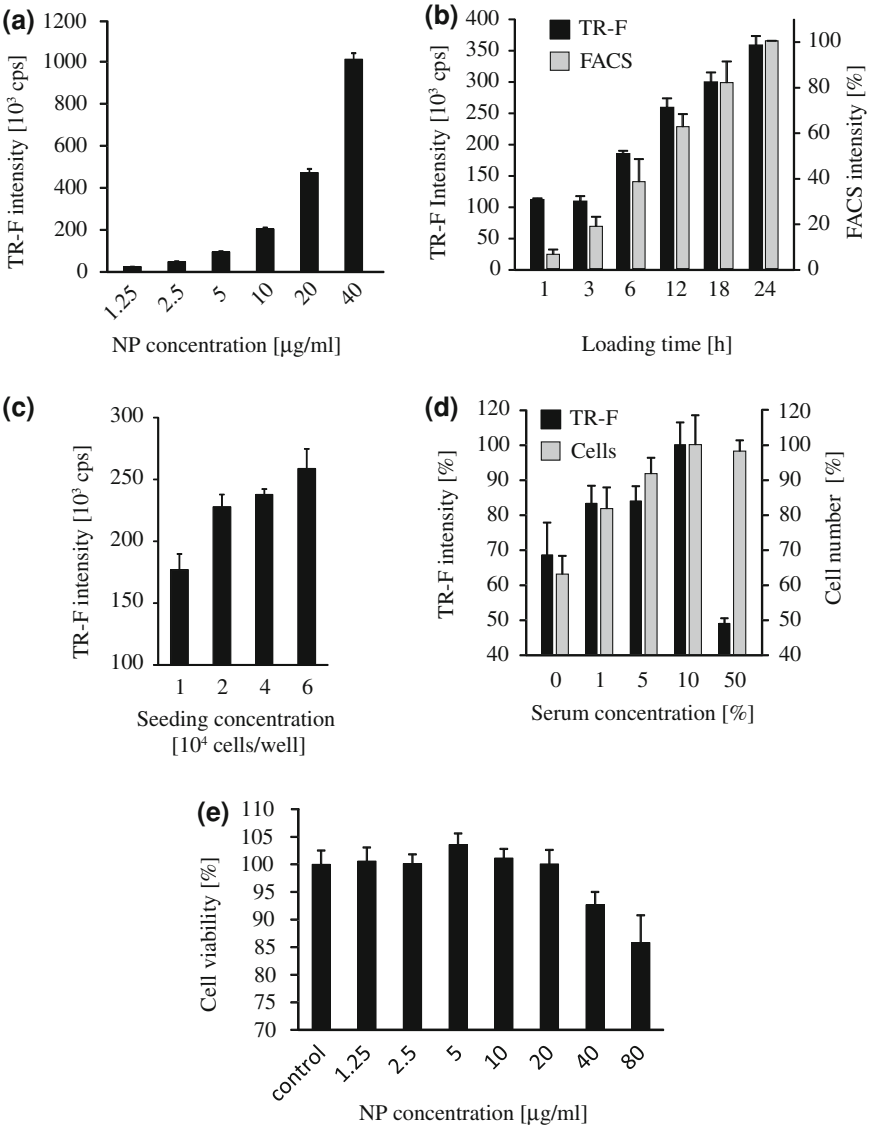

Fig. 2.14 Loading of NanO2 probe in MEF cells in DMEM medium, 37 °C. **a–d** The dependence of TR-F intensity signals on the probe concentration (**a**, for 12 h loading), loading time (**b**, for 10 µg/mL probe), cell seeding concentration (**c**) and serum content in the medium (**d**). **e**. The effects of probe on cell viability (15 h loading). Adapted with permission from [10]. Copyright 2011, American Chemical Society

atmosphere or cellular hypoxia can be performed with reduced cell numbers or lower probe loading, as compared to normoxic (ambient air) conditions.

(4) Medium composition, mainly serum content and the presence of various additives (e.g. transfection reagents or compounds that have an effect on cell membrane and endocytosis processes.
(5) Toxicological impact of the probe on cells which may result in cell death and loss of integrity, thus releasing the icO_2 probe into bulk medium. These effects have to be carefully analysed at the start of each study with a new model and monitored throughout the work.

2.3.3 Probe Calibration

Reliable calibration is key to successful and accurate sensing of O_2 by phosphorescence quenching. Particularly when performing O_2 calibrations of icO_2 probes, it is necessary to consider all the main factors that can potentially influence measured lifetime values and the O_2 concentrations calculated from these values. Although phosphorescence lifetime is the intrinsic parameter of the probe, its measurement may be affected by: (i) instrumental factors which include measurement errors and systematic inaccuracy originating from the instrument hardware or software; (ii) changes in probe micro-environment; (iii) calibration set-up and operator errors; (iv) errors in converting lifetime values into O_2 concentration.

It is, therefore, recommended to perform the calibration in conditions that closely resemble those used in the biological experiments, including the instrument, probe localisation, optical alignment, intensity signals, data acquisition and processing algorithms, O_2 concentration range. Although some icO_2 probes (e.g. nanoparticle based) are shielded from quenching interferences and effects of changing microenvironment, variability in lifetime readings can be still observed when the same O_2 probe is measured on different instruments or in different cell types. Some of the commercial instruments (claimed to be suitable for sensitive TR-F measurements), in fact, show a large variability and inaccuracy of measured lifetime and a pronounced intensity dependence. Such instruments are therefore not suitable for quantitative O_2 sensing experiments.

To precisely control O_2 in the microplate compartment, the instrument should have a built-in O_2 controller (e.g. FLUOstar Omega, BMG Labtech). Standard TR-F readers such as Victor, PerkinElmer can be placed in a hypoxia chamber with O_2 control (e.g. Coy Laboratory Products, MI). When calibrations are performed with standard gas mixtures in a hypoxia chamber, correction for variations in atmospheric pressure should be made. For example, at normal atmospheric pressure (1 Bar or 760 mmHg), 10.0 % v/v O_2 in hypoxia chamber corresponds to partial pressure of 10.0 kPa O_2 or dissolved concentration 100 μM.

Based on our experience with different icO_2 probes, the following calibration procedure is recommended:

(1) Seed test cells in multiple wells of a microplate and culture them to medium/high confluence;

(2) Load the cells with probe in standard growth medium, to achieve sufficiently high TR-F intensity signals in ambient air environment that ensure reliable lifetime measurements (see above typical thresholds). Include wells with unloaded cells as blanks;
(3) Add Ant A to the cells (5–10 μM) to inhibit cellular respiration and bring cellular O_2 to the levels in bulk medium. This requires ~15 min incubation.
(4) Insert the plate with cells in the reader pre-equilibrated at the desired temperature (normally 37 °C) and atmospheric O_2 (can start with ambient, 20.9 %).
(5) Initiate ratiometric TR-F measurements in kinetic mode monitoring probe signal in assay wells every 5–10 min for about 20–40 min until stable intensity and lifetime readings are achieved. This corresponds to gas and temperature equilibration of samples in the well.
(6) Change atmospheric O_2 -level and repeat the monitoring cycle. Make this step at several O_2 levels covering the range of interest, for example, 20.9 %, 15.0 %, 10.0 %, 5.0 %, 3.0 % and 1.0 % O_2.
(7) In the end of the protocol add glucose oxidase and β-D-glucose to the samples (50 μg/ml and 10 mM, respectively) and measure lifetimes as above for fully deoxygenated samples (zero O_2 point).
(8) Calculate lifetimes for the plateau region for each O_2 level. For several wells and measurement points determine average lifetime values and standard deviations.
(9) Use these data points to plot a calibration graph. Perform best fit of the data points to determine the calibration function (mathematical equation): $[O_2] = f(\tau)$.

Representative experimental data, O_2 calibration graph and analytical function derived from them, are shown in Fig. 2.15. Figure 2.15a also shows that in the respiring MEF cells measured lifetime values are significantly higher and O_2 levels lower than the standards, so they cannot be used for the calibration. During the prolonged calibration measurement gradual evaporation of medium should be compensated by adding water to the samples when the level drops below 50 %.

2.3.4 Control of Oxygenation in Cultures of Adherent Cells

The model presented in Sect. 2.3.1 and Fig. 2.13 suggests that actively respiring cells can partly or fully deoxygenate themselves and generate O_2 gradients that propagate across the sample. Deoxygenation due to intrinsic respiration (cells are acting as O_2 sinks) is particularly important for actively respiring cells and cells cultured under reduced atmospheric O_2 levels. Figure 2.16 shows lifetime and icO_2 profiles monitored on a TR-F reader in the resting MEFs seeded at different density on 96-well plate, grown for 12 h at 20.9 % O_2 and then transferred to 3 % O_2. The initial portion of the curve (0–45 min) reflects the establishment of new

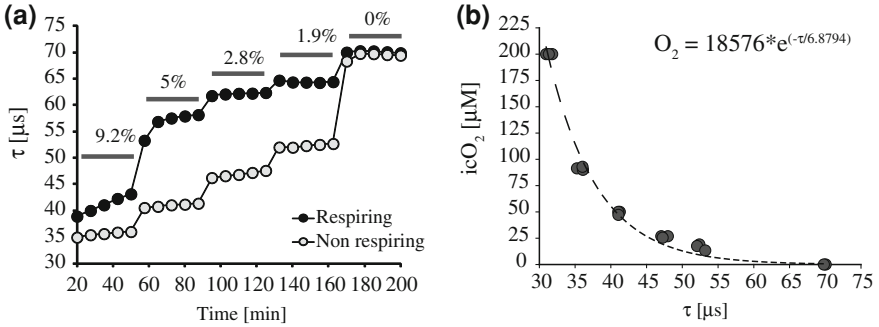

Fig. 2.15 Calibration of the NanO2 probe in MEF cells generated on Victor4 TR-F reader and hypoxia chamber (glove box, Coy Laboratory Products) at 37 °C. A. Experimental steps of the probe calibration between 9.2 % and 0 % atmospheric O_2. Oxygenation of respiring cells is also shown. B. Analytical equation for calculating O_2 concentration (µM), produced by fitting the data points (3 independent experiments) with exponential function

steady state between O_2 consumption and supply, which is characteristic for particular atmospheric O_2 level and respiratory activity of the sample.

These results show that respiring cells in static culture do deoxygenate themselves and can easily become anoxic when O_2 availability decreases (hypoxia). Inhibition of respiration by Ant A eliminates this effect while the cells still remain viable (ATP levels unaffected) due to the compensatory activation of glycolysis outlined above. At 20.9 % atmospheric O_2 oxygenation of MEFs seeded at the same density varies between $\sim$180 µM (10^4 cells) and $\sim$140 µM (5×10^4 cells). Similar profiles of cellular O_2 are expected for tissue culture flasks maintained under static conditions at which steady-state O_2 gradients are also generated. These O_2 gradients can be disrupted by agitation or shaking the flasks and microplates.

The critical observation to draw from these data is that precise O_2 levels set in the hypoxia chamber (e.g. 0.5 %, 1.0 % or 5.0 %) do not translate into the same O_2 levels within the cells. Such a relationship only holds at very low cell densities. Therefore, careful control of experimental conditions is required to avoid extreme fluctuations in cellular oxygenation.

2.3.5 *Effects of Cell Metabolic Activity on icO_2*

Besides atmospheric O_2, cellular respiratory activity (parameter *k* in the model and Eqs. 2.1, 2.2) also has a large effect on icO_2, and this can be explored to study changes in cell metabolism, compare different cell types or mutant cells, apply drug treatments and investigate mechanism of action. Thus, Fig. 2.17 shows that Krebs cycle deficient MEFs (see Sect. 2.2.4 and [41]), when transferred from normoxia to moderate hypoxia (8 % O_2), have a much higher deoxygenation rate than WT MEFs. Parallel measurement of cells sealed under oil with an ecO_2 probe

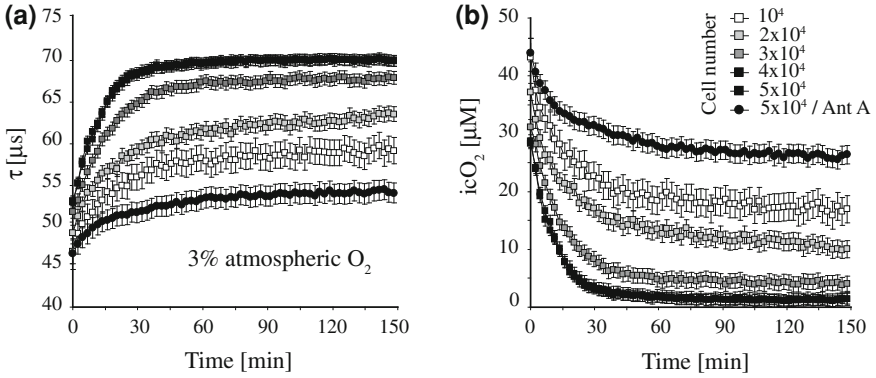

Fig. 2.16 Measured lifetime (**a**) and calculated O_2 (**b**) profiles for resting MEFs cultured in DMEM medium at different seeding densities (*indicated*). Experiment was performed using NanO2 probe under 3 % atmospheric O_2 at 37 °C

confirmed that OCR in KO cells was much lower and did not increase in the presence of FCCP.

Similarly, treatment of the cells with drugs that target cell metabolism can have a profound influence: an increase in icO_2 (or reduction in probe lifetime) points to the inhibition of cell respiration, whereas reduction in icO_2—to the activating/uncoupling effect. For example, treatment of PC12 cells with a well-known inhibitor of V-ATPase and K^+ ionophore Bafilomycin A (Baf) [60], [61] revealed its pronounced effect as a mitochondrial uncoupler [15]. This was seen as a reduction of icO_2 even under ambient atmosphere (20.9 % O_2) which occurs in a dose and time-dependent manner.

In MEFs, the respiratory response to Baf was also dose dependent and in normoxia became significant at ≥0.25 µM Baf (Fig. 2.18a) without significant effect on cellular ATP levels. Since relative deoxygenation of respiring cells increases with decreased O_2 availability [59], in agreement with this rule at 6 % atmospheric O_2 the effect of Baf became more pronounced and detectable already at concentration 0.06 µM (Fig. 2.18b), while 0.2–0.5 µM Baf caused a sustained decrease in icO_2 down to 1–5 µM. An increase in cell respiration was linked to significant changes in mitochondrial function (Fig. 2.19). Thus, average intensity of TMRM (probe for mitochondrial membrane potential, ΔΨm) was partially decreased and the analysis of co-localization of TMRM and $_{mito}$Case12 (non-leaking mitochondria-targeted Ca^{2+}-biosensor) revealed continuous flickering of ΔΨm. The behaviour of MEF cells and effects caused by Baf were similar to what was previously found in PC12 cells and described in greater detail elsewhere [15].

Cell deoxygenation induced by Baf can be abolished by the addition of Ant A. After such double treatment cellular ΔΨm and ΔpH_m rapidly disappeared, since complex III could not contribute to their restoration, while FoF1 ATP-synthase consumed glycolytic ATP to pump protons outside the matrix. Inhibition of

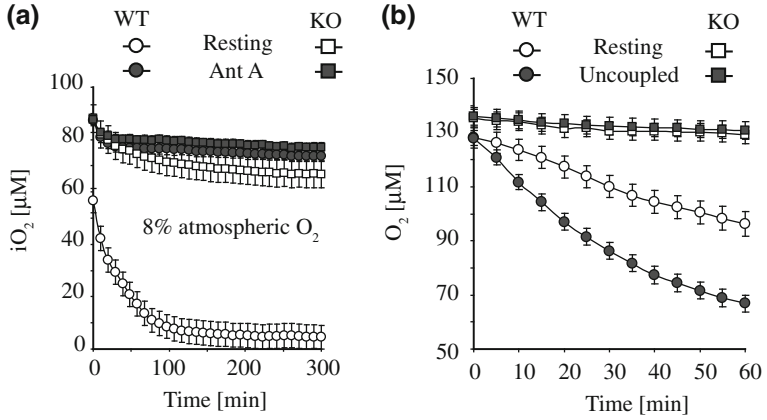

Fig. 2.17 The effects of respiration activity and metabolic status of the WT and FH deficient MEF cells on icO_2 (**a**) and their correlation with the OCR measured with an extracellular probe under oil seal (**b**)

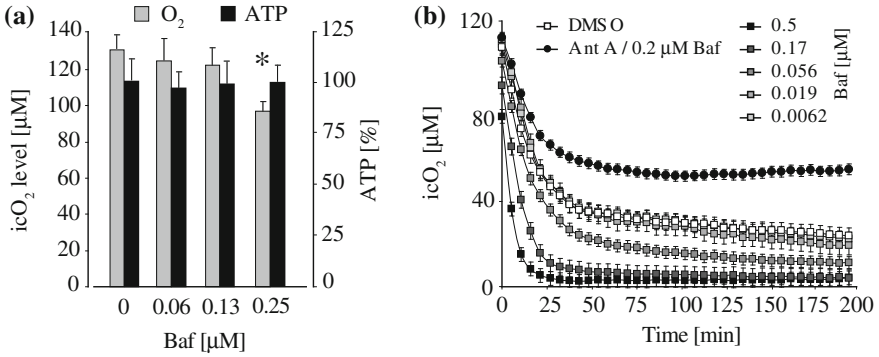

Fig. 2.18 Uncoupling effect of Baf on icO_2 and ATP levels in MEF cells. **a** At normoxia (21 % O_2) treatment with 0.25 μM Baf causes significant reduction in icO_2 and does not affect cellular ATP levels. **b** In hypoxia (6 % atmospheric O_2) the effect of Baf on icO_2 levels is seen at >0.056 μM concentrations. Deep deoxygenation of MEFs lasts for several hours. In all cells treated with Ant A (10 μM) the O_2 does not differ from atmospheric level due to inhibition of the mitochondrial complex III. Asterisks indicate significant difference from mock control (DMSO)

respiration is, therefore, extremely stressful for the cells. However, physiological feedback mechanisms that exist in the cell, such as nitric oxide (NO) signalling, can regulate the respiratory responses and cell oxygenation. In the presence of NO the cells cannot deoxygenate themselves below a certain level. This is because NO effectively competes with O_2 for cytochrome *c* oxidase (mitochondrial complex IV) and inhibits its activity and at reduced O_2 availability decreases cell respiration to a certain level in a manner dependent on cellular O_2 and NO concentrations [59]. Figure 2.20a demonstrates that in the presence of NO donor DETA-NONOate (1 mM), which maintains ~0.5 μM NO in the medium, respiration was

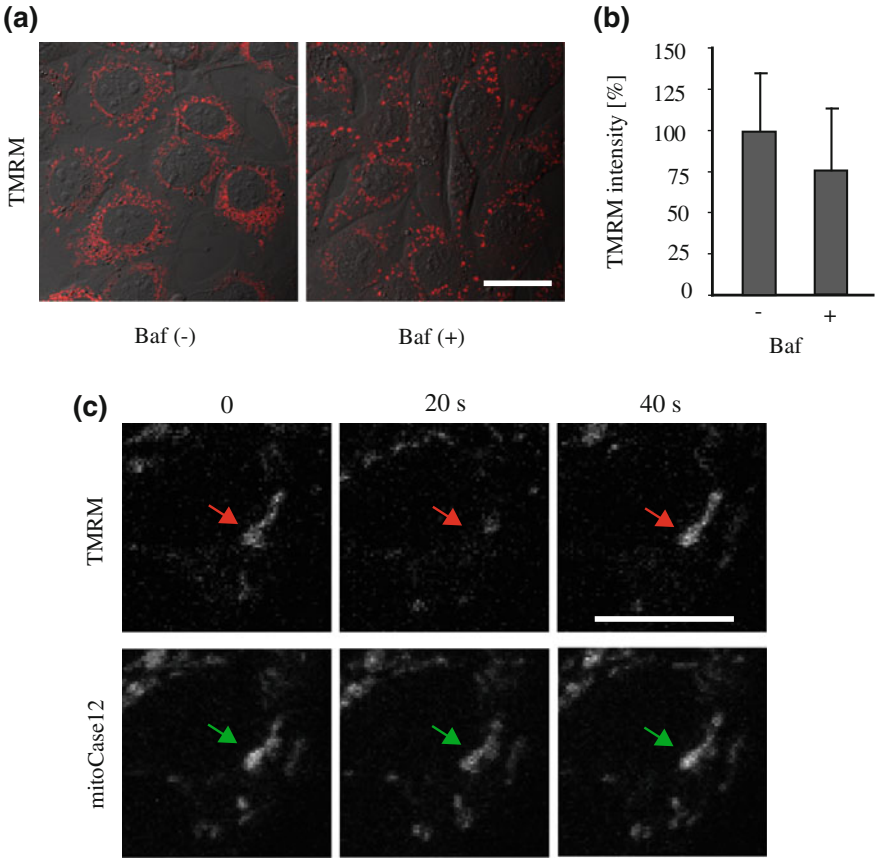

Fig. 2.19 Effect of Baf treatment on the ΔΨm polarisation in MEFs. **a** Baf treatment (0.25 μM for 45–60 min) causes slight depolarisation of the ΔΨm, as monitored using TMRM. **b** Semi-quantitative analysis of TMRM fluorescence intensity is shown in (**a**). **c** Baf induces random flickering of the ΔΨm with an average frequency of 20 s (*red arrow*), as seen in the single mitochondrion visualised with a mitochondrial Ca^{2+} sensor mitoCase12 (*green arrow*). Scale bar represents 20 μm

inhibited when O_2 levels drop to about 20–25 μM. Cellular ATP levels remains steady and independent of the treatment with Baf and DETA-NONOate (Fig. 2.20b). At ~4.5 % atmospheric O_2, such inhibition of respiration occurs regardless of Baf treatment, demonstrating universality of NO signaling.

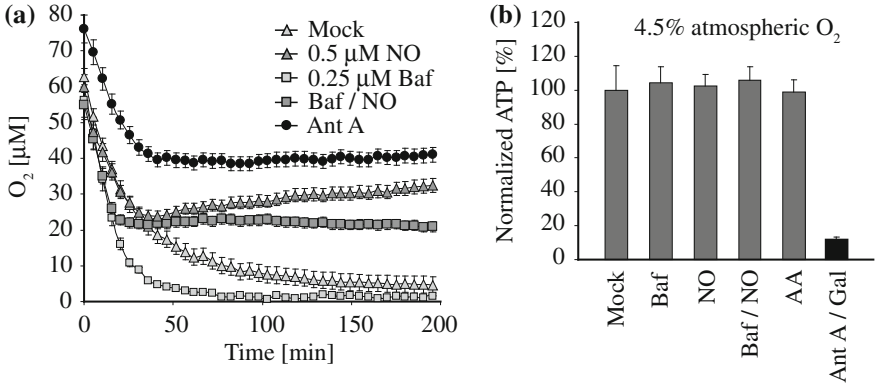

Fig. 2.20 Effect of NO on the respiratory response to Baf of differentiated PC12 cells monitored at 4.5 % O_2. **a** Cell deoxygenation profiles. **b** The levels of cellular ATP

2.3.6 Multiple Treatments with Drugs and Monitoring of Transient Responses of Cells

As icO_2 concentration is a function of O_2 availability, conditions of mass exchange and cell respiratory activity, its levels may be affected significantly by rapid metabolic stimulation whereby a transient imbalance between O_2 supply and demand leads to a rapid local decrease in icO_2 ('overshoot effect' [59]). Even a short, transient increase in respiration may lead to sustained deoxygenation, imposing an energy stress which can in turn trigger cell adaptation to hypoxia. The latter can be seen, for example, as a shift in energy production from OxPhos to glycolysis, activation of hypoxia inducible factor (HIF) pathway and change in gene expression profile [59]. When measured in icO_2 or lifetime scale, the shape of cellular responses to metabolic stimulation is determined by the type of cells, their physiological environment (growth medium, supplements, etc.), mode of drug action and diffusion characteristics of the measurement platform. By changing experimental conditions such as, the volume of medium, atmospheric O_2 or temperature, one can modulate the observed response and extract specific mechanistic information about cellular function. For example, rapid depletion of extracellular Ca^{2+} (eCa^{2+}) with EGTA was shown to cause transient elevation of respiration in PC12 cells, through Na^+ influx and a subsequent increase in mitochondrial Na^+/Ca^{2+} and H^+/Na^+ exchange [17]. EGTA also slightly decreased the respiratory response to subsequent plasma membrane depolarisation by KCl [16, 17]. Based on this knowledge, we investigated how the depletion of eCa^{2+} affects the response to FCCP uncoupling.

PC12 cells pre-incubated in glucose(+) and galactose(+) media for 3 h and were treated sequentially with 5 mM EGTA and 1 µM FCCP (Fig. 2.21). Glucose(+) cells exhibited higher resting icO_2 than galactose(+) cells, and a lower response to FCCP which was slightly inhibited by eCa^{2+} depletion. In galactose(+) medium for

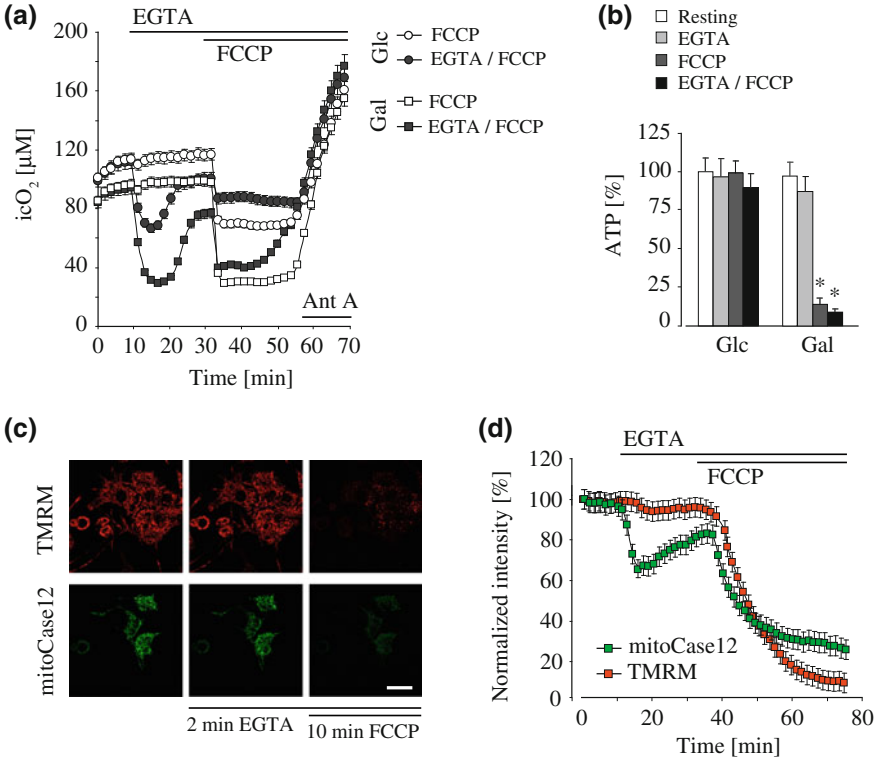

Fig. 2.21 Effect of eCa^{2+} chelation on the respiratory response of PC12 cells to FCCP. **a** Real-time profiles of icO_2. Replacement of glucose with galactose activates basal respiration and respiratory responses of the cells. Chelation of eCa^{2+} with 5 mM EGTA transiently increases cellular respiration. In eCa^{2+}-free conditions the response to mitochondrial uncoupling is reduced. Ant A inhibits respiration in all the samples and re-oxygenate the cells. **b** ATP levels measured at the peak of the response to FCCP (50 min) show a dramatic decrease in the absence of glycolytic ATP flux upon uncoupling. **c** Confocal images and **d** time profiles of TMRM and mitoCase12 fluorescence demonstrate the changes in $\Delta\Psi m$ and $mitoCa^{2+}$ upon EGTA and FCCP treatment in glucose(+) medium. Asterisks indicate significant difference. Scale bar represents 20 µm

cells treated with EGTA, the increase in respiration in response to FCCP was transient and followed by rapid reoxygenation of the cells reflecting their loss of respiratory activity. FCCP treatment caused a large drop in cellular ATP in galactose(+) medium, but not in glucose(+) (Fig. 2.21b). Interestingly, in the presence of eCa^{2+} the response to FCCP was more sustained suggesting that ATP levels are not critical for cell respiration. In the cells incubated on glucose and producing ATP via both glycolysis and OxPhos, the FCCP-specific increase in respiration was more sustainable, regardless of eCa^{2+}. Parallel confocal microscopy analysis revealed that depletion of eCa^{2+} caused a moderate decrease in $mitoCa^{2+}$ and only minor changes in $\Delta\Psi m$, whereas treatment with FCCP caused massive release of $mitoCa^{2+}$ and complete dissipation of $\Delta\Psi m$ (Fig. 2.21c,d). Pre-treatment with Ant A inhibited respiratory responses in all the samples.

2.4 Instrument Requirements and Selection Criteria

A wide variety of plate reader types are currently used in conjunction with extracellular probes for the analysis of cellular oxygen consumption [1, 5, 11, 20, 26, 31, 59, 62]. Such measurements are typically performed in prompt fluorescence mode or in TR-F mode. The advantage of the latter is that interference from autofluorescent components and optical properties of the test sample can be minimised significantly thereby providing superior signal to blank values and more stable readings. However, time resolution of such instruments is typically limited by the Xe-flashlamp used as excitation light source whereby the 'tail' is often still detectable at a delay of 20 μs while the emission lifetime of the probes themselves sets an upper limit on the delay time that can be used. A 30 μs delay is, therefore, recommended as an optimum value [11]. Another relevant consideration for TR-F readers is that detection is generally PMT based and which can be insensitive above 650 nm, although this is only problematic where probe signal is limited. The efficiency of plate heating can also be important, particularly when an entire microplate is being measured. Some instruments show a temperature differential across the plate whereby the centre of the plate is at a slightly lower temperature to the edge. Since both probe response and cell respiration are temperature sensitive, such temperature disparity can result in an 'edge effect'. This effect becomes less pronounced as one moves from 37 °C to 30 °C. Onboard data processing software also varies significantly across models. On some models, all data analyses and subsequent reductions can be done automatically on the plate reader software while in other extreme cases all data have to be exported to discrete package such as MS Excel for subsequent manual processing.

While an intensity-based measurement approach can be applied to certain extracellular oxygen measurements, the investigation of intracellular oxygen, extracellular pH or more quantitative extracellular oxygen consumption analysis, requires the RLD approach to lifetime determination outlined in Chap. 1. For this measurement mode, the choice of instrument is critical as both the lamp used and the S:B values achievable determine measurement success. In this regard, we have found Victor (PerkinElmer, Finland] and FLUOstar or POLARstar Omega™ (BMG Labtech, Germany) to provide best performance with other, often higher end readers not showing the requisite performance. The addition of an Atmospheric Control Unit (ACU) to the FLUOstar Omega™ allowing modulation of O_2 and CO_2 in the measurement chamber adds additional functionality which is particularly relevant to icO_2 investigations. These instruments work well with PtCP- and PtPFPP-based probes including MitoXpress®, nanoparticles [10] and peptide conjugates [13] and are now used in the high-throughput assessment of O_2 in cell populations and other sample types. It also worth noting that, while this measurement approach is applicable to Pt-Porphyrin-based probes, it is far less successful in the measurements with Ru(II) complexes due to their short lifetime. Longwave O_2 probes emitting in the very-near infrared region can also be problematic for standard readers which are rather insensitive at >700 nm. There are

Table 2.2 Pt-porphyrin O_2 probe signals from samples with mammalian cells in standard 96-well plates measured across different instruments using recommended probe concentrations and settings optimised for kinetic analysis. These are indicative values as intensity signals can vary from instrument to instrument

Instrument	Probe	Intensity signals 1, 2[a]	Blanks 1, 2[a]	S:B	Measured lifetime, μs
Omega (BMG)	MitoXpress® (EC)	50,000/14,000	5,000/400	10/35	23.1 ± 0.5
	NanO2 (IC)	55,000/15,500	2,500/400	22/39	30.2 ± 0.5
Victor[4] (PerkinElmer)	MitoXpress® (EC)	150,000/26,800	700/265	210/120	23.2 ± 0.2
	NanO2 (IC)	150,000/40,100	700/265	210/145	30.3 ± 0.2
Genius Pro (Tecan)[b]	MitoXpress® (EC)	600	25	24	n/a
Spectramax[c] (Molecular Devices)	MitoXpress® (EC)	65	15	5	n/a

[a] Under optimised instrument settings and RLD delay times 30 and 70 μs, at 37 °C in air-saturated solution and optimised probe concentrations
[b] Instrument only supports TR-F, but not RLD mode
[c] can only measure Pt-porphyrins in prompt fluorescence mode
n/a—not applicable

also instances where instruments have been custom designed specifically for such applications and Pt-porphyrin labels [63].

Typical performance characteristics of several commercial fluorescent readers are summarised in Table 2.2. One can see that intensity signals and S:B ratio vary significantly from one instrument to another. Using non-optimal instruments, measurement and RLD settings may lead to a significant loss of performance of phosphorescence lifetime and O_2 concentration determination (inaccurate values, large S.D.). When analysing large number of samples on one plate, scanning speed of the instrument should be considered. On the first three instruments, one scan of a 96-well plate normally takes about 2 min. To increase measurement frequency (sampling time for each well), one can reduce the number of samples on the plate or change measurement settings (some loss of sensitivity may occur). Overall, for O_2 measurement with Pt-porphyrin probes strong preference is given to high sensitivity TR-F readers.

2.5 Conclusions

Overall, optical O_2 sensing using fluorescent and TR-F plate-reader detection represents a powerful and versatile technique for assessment of respiratory responses in cell populations. It also provides an experimental platform for the development and characterisation of new extracellular and intracellular O_2 probes, and facilitates the analysis of both O_2 concentrations and localised oxygen gradients. The utility of the technology is underscored by the spectrum of applications and experimental data described above demonstrating that optical O_2 sensing measurements performed on standard fluorescent/TR-F plate readers provide

valuable information on the OCR, metabolic status, cell oxygenation and cellular responses to metabolic stimulation. Populations of cells in small samples placed in microtiter plates or other substrates can be measured in a simple, fast and high-throughput manner providing quantitative and statistically sound data. The choice of different measurement formats and detection modalities (described in Chap. 1) and the high degree of flexibility of such systems makes them well-suited for the analysis of cells systems and diverse biological and animal models under various external O_2 levels, metabolic stimulation or stress. Measurement can be performed in standard platforms such as microtiter plates or in customised systems such as capillary cuvettes, cell-based biochips and microfluidic systems. Experimental set-ups are relatively straightforward and do not require highly specialised instrumentation, and are therefore broadly applicable across biological science even by the researchers without special skills or previous experience with optical O_2 sensing. A large number of academic and industrial labs have already adopted the technology for routine use in their research and screening.

In all these applications, modern TR-F readers usually provide high sensitivity in detecting the probes based on Pt-porphyrin dyes. However, not all instruments and probes can be used with the same degree of success. Instrument and probe must be mutually compatible whereby appropriate, spectral characteristics, time resolution, sensitivity, temperature control and measurement consistency must be achieved. Additional factors such as data processing software can also be important considerations when designing the experimental set-up.

Phosphorescent signals obtainable with the new generation icO_2 probes such as NanO2 can be as high as the signals with the extracellular probes. These probes give the user a considerable signal window to perform reliable and accurate lifetime-based O_2 and OCR measurements which can then be related to cell and sample parameters. Also these probes do not cause any significant cell damage or impact on cellular function. In some applications, even simple intensity-based fluorescent readers can provide very satisfactory analytical performance in measuring relative OCRs and relative oxygenation and changes in cell/sample respiration, however, lifetime-based O_2 sensing remains a preferred option.

Quantitative data generated in this manner with adherent cell cultures, icO_2 probes can be allied to a suite of additional functional bioassays providing a data set of high physiological relevance and giving more complete picture of cellular metabolic responses. The open microplate format used in icO_2 measurements allows multiple treatments to be applied in one experiment while tracing changes in icO_2 and cell respiration in real time. This is very useful for various mechanistic studies, when the interplay of different drugs, conditions and processes within the cell can be analysed. Moreover, phosphorescent O_2 sensing probes have high potential for multiplexing, and O_2 analyses can be coupled with parallel measurement of other cellular parameters, including ATP and NAD(P)H, cytosolic and mitochondrial Ca^{2+} and pH, the $\Delta\Psi m$ and redox state. This can again provide a more in-depth and detailed insight in cell metabolism and bioenergetics.

The two main approaches to O_2 measurement and corresponding set-ups complement each other. Thus, measurements with extracellular probes are usually

conducted under oil overlay (i.e. partially sealed samples), in a kinetic assay which lasts 15–90 min producing one OCR value per sample. Effectors and treatments have to be applied prior to the assay, since additions during the measurement are inconvenient due to the oil seal. In contrast, O_2 measurements with intracellular probes are carried out in an open system (liquid sample is exposed to gaseous atmosphere), when repeatable additions of multiple effectors is applicable.

The format used for icO_2 measurement (see Sect. 2.3.1 and Fig. 2.13) resembles the tissue and blood vessel system of living organisms. Therefore, the processes observed in such assays (partial deoxygenation, dysbalance between O_2 utilization and supply) may also occur in vivo in a number of common (patho)physiological conditions such as ischemia and reperfusion, stroke, neuronal excitotoxicity, i.e. when certain areas remote from the source of O_2 undergo metabolic stress or activation, and also in cancer and embryo development. O_2 diffusion in tissue is thought to be similar to that of water, growth media and extracellular fluid [8, 64]. Characterisation of 3D O_2 gradients is, however, a more complicated task and requires specialised techniques, such as O_2 imaging microscopy described in Chap. 3. For larger specimens such as tissue sections and organs, this is even more challenging since optical techniques have limited penetration into tissue. These O_2 sensing techniques, therefore, have the potential to provide new insights into cellular function, mechanism of drug actions and even the examination of therapeutic targets and disease progression, particularly where mitochondria, metabolism or oxygen availability are central players.

Acknowledgments This work was supported by the Science Foundation Ireland, grant 07/IN.1/B1804, and the EU FP7 project Chebana MC-IAPP-2009-230641.

References

1. Hynes J, Floyd S, Soini AE, O'Connor R, Papkovsky DB (2003) Fluorescence-based cell viability screening assays using water-soluble oxygen probes. J Biomol Screen 8:264–272
2. O'Riordan TC, Buckley D, Ogurtsov V, O'Connor R, Papkovsky DB (2000) A cell viability assay based on monitoring respiration by optical oxygen sensing. Anal Biochem 278:221–227
3. Schouest K, Zitova A, Spillane C, Papkovsky D (2009) Toxicological assessment of chemicals using Caenorhabditis elegans and optical oxygen respirometry. Environ Toxicol Chem 28:791–799
4. Zitova A, O'Mahony FC, Cross M, Davenport J, Papkovsky DB (2009) Toxicological profiling of chemical and environmental samples using panels of test organisms and optical oxygen respirometry. Environ Toxicol 24:116–127
5. Alderman J, Hynes J, Floyd SM, Krüger J, O'Connor R, Papkovsky DB (2004) A low-volume platform for cell-respirometric screening based on quenched-luminescence oxygen sensing. Biosens Bioelectron 19:1529–1535
6. Zitova A, Hynes J, Kollar J, Borisov SM, Klimant I, Papkovsky DB (2010) Analysis of activity and inhibition of oxygen-dependent enzymes by optical respirometry on the LightCycler system. Anal Biochem 397:144–151
7. O'Donovan C, Twomey E, Alderman J, Moore T, Papkovsky D (2006) Development of a respirometric biochip for embryo assessment. Lab Chip 6:1438–1444

8. Wilson DF (2008) Quantifying the role of oxygen pressure in tissue function. Am J Physiol Heart Circ Physiol 294:H11–H13
9. O'Riordan TC, Fitzgerald K, Ponomarev GV, Mackrill J, Hynes J, Taylor C, Papkovsky DB (2007) Sensing intracellular oxygen using near-infrared phosphorescent probes and live-cell fluorescence imaging. Am J Physiol Regul Integr Comp Physiol 292:R1613–1620
10. Fercher A, Borisov SM, Zhdanov AV, Klimant I, Papkovsky DB (2011) Intracellular O2 Sensing Probe Based on Cell-penetrating Phosphorescent Nanoparticles. ACS Nano 5:5499–5508
11. O'Riordan TC, Zhdanov AV, Ponomarev GV, Papkovsky DB (2007) Analysis of intracellular oxygen and metabolic responses of mammalian cells by time-resolved fluorometry. Anal Chem 79:9414–9419
12. Dmitriev RI, Papkovsky DB (2012) Optical probes and techniques for O(2) measurement in live cells and tissue. Cell Mol Life Sci [Epub ahead of print]
13. Dmitriev RI, Ropiak HM, Yashunsky DV, Ponomarev GV, Zhdanov AV, Papkovsky DB (2010) Bactenecin 7 peptide fragment as a tool for intracellular delivery of a phosphorescent oxygen sensor. FEBS J 277:4651–4661
14. Dmitriev RI, Zhdanov AV, Ponomarev GV, Yashunski DV, Papkovsky DB (2010) Intracellular oxygen-sensitive phosphorescent probes based on cell-penetrating peptides. Anal Biochem 398:24–33
15. Zhdanov AV, Dmitriev RI, Papkovsky DB (2011) Bafilomycin A1 activates respiration of neuronal cells via uncoupling associated with flickering depolarization of mitochondria. Cell Mol Life Sci 68:903–917
16. Zhdanov AV, Ward MW, Prehn JH, Papkovsky DB (2008) Dynamics of intracellular oxygen in PC12 Cells upon stimulation of neurotransmission. J Biol Chem 283:5650–5661
17. Zhdanov AV, Ward MW, Taylor CT, Souslova EA, Chudakov DM, Prehn JH, Papkovsky DB (2010) Extracellular calcium depletion transiently elevates oxygen consumption in neurosecretory PC12 cells through activation of mitochondrial Na(+)/Ca(2 +) exchange. Biochim Biophys Acta 1797:1627–1637
18. Hynes J, O'Riordan TC, Zhdanov AV, Uray G, Will Y, Papkovsky DB (2009) In vitro analysis of cell metabolism using a long-decay pH-sensitive lanthanide probe and extracellular acidification assay. Anal Biochem 390:21–28
19. Hynes J, Marroquin LD, Ogurtsov VI, Christiansen KN, Stevens GJ, Papkovsky DB, Will Y (2006) Investigation of drug-induced mitochondrial toxicity using fluorescence-based oxygen-sensitive probes. Toxicol Sci 92:186–200
20. O'Mahony F, Green RA, Baylis C, Fernandes R, Papkovsky DB (2009) Analysis of total aerobic viable counts in samples of raw meat using fluorescence-based probe and oxygen consumption assay. Food Control 20:129–135
21. Hynes J, Hill R, Papkovsky DB (2006) The use of a fluorescence-based oxygen uptake assay in the analysis of cytotoxicity. Toxicol in Vitro 20:785–792
22. Will Y, Hynes J, Ogurtsov VI, Papkovsky DB (2007) Analysis of mitochondrial function using phosphorescent oxygen-sensitive probes. Nat. Protocols 1:2563–2572
23. Yao J, Irwin R, Chen S, Hamilton R, Cadenas E, Brinton RD (2011) Ovarian hormone loss induces bioenergetic deficits and mitochondrial beta-amyloid. Neurobiol Aging 6(7):e21788
24. Hu L-F, Lu M, Tiong CX, Dawe GS, Hu G, Bian J-S (2010) Neuroprotective effects of hydrogen sulphide on Parkinson's disease rat models. Aging Cell 9:135–146
25. Chan DC (2006) Mitochondria: dynamic organelles in disease aging, and development. Cell 125:1241–1252
26. Marroquin LD, Hynes J, Dykens JA, Jamieson JD, Will Y (2007) Circumventing the Crabtree effect: replacing media glucose with galactose increases susceptibility of HepG2 cells to mitochondrial toxicants. Toxicol Sci 97:539–547
27. Kettenhofen R, Bohlen H (2008) Preclinical assessment of cardiac toxicity. Drug Discov Today 13:702–707

28. Choubey V, Safiulina D, Vaarmann A, Cagalinec M, Wareski P, Kuum M, Zharkovsky A, Kaasik A (2011) Mutant A53T α-synuclein induces neuronal death by increasing mitochondrial autophagy. J Biol Chem
29. O'Hagan KA, Cocchiglia S, Zhdanov AV, Tambuwala MM, Cummins EP, Monfared M, Agbor TA, Garvey JF, Papkovsky DB, Taylor CT, Allan BB (2009) PGC-1alpha is coupled to HIF-1alpha-dependent gene expression by increasing mitochondrial oxygen consumption in skeletal muscle cells. Proc Natl Acad Sci U S A 106:2188–2193
30. Favre C, Zhdanov A, Leahy M, Papkovsky D, O'Connor R (2010) Mitochondrial pyrimidine nucleotide carrier (PNC1) regulates mitochondrial biogenesis and the invasive phenotype of cancer cells. Oncogene 29:3964–3976
31. Hynes J, Swiss RL, Will Y (2012) High-throughput analysis of mitochondrial oxygen consumption. Methods Mol Biol 810:59–72
32. Sung HJ, Ma W, Wang PY, Hynes J, O'Riordan TC, Combs CA, McCoy JP Jr, Bunz F, Kang JG, Hwang PM (2010) Mitochondrial respiration protects against oxygen-associated DNA damage. Nat Commun 1:5
33. Jonckheere AI, Huigsloot M, Janssen AJ, Kappen AJ, Smeitink JA, Rodenburg RJ (2010) High-throughput assay to measure oxygen consumption in digitonin-permeabilized cells of patients with mitochondrial disorders. Clin Chem 56:424–431
34. Kelm JM, Lorber V, Snedeker JG, Schmidt D, Broggini-Tenzer A, Weisstanner M, Odermatt B, Mol A, Zünd G, Hoerstrup SP (2010) A novel concept for scaffold-free vessel tissue engineering: self-assembly of micro tissue building blocks. J Biotechnol 148:46–55
35. Amacher DE (2005) Drug-associated mitochondrial toxicity and its detection. Curr Med Chem 12:1829–1839
36. Lin MT, Beal MF (2006) Mitochondrial dysfunction and oxidative stress in neurodegenerative diseases. Nature 443:787–795
37. Muller WE, Eckert A, Kurz C, Eckert GP, Leuner K (2011) Mitochondrial dysfunction: common final pathway in brain aging and Alzheimer's disease–therapeutic aspects. Mol Neurobiol 41:159–171
38. Bartlett K, Eaton S (2004) Mitochondrial beta-oxidation. Eur J Biochem 271:462–469
39. Tennant DA, Duran RV, Gottlieb E (2010) Targeting metabolic transformation for cancer therapy. Nat Rev Cancer 10:267–277
40. Wise DR, DeBerardinis RJ, Mancuso A, Sayed N, Zhang XY, Pfeiffer HK, Nissim I, Daikhin E, Yudkoff M, McMahon SB, Thompson CB (2008) Myc regulates a transcriptional program that stimulates mitochondrial glutaminolysis and leads to glutamine addiction. Proc Natl Acad Sci U S A 105:18782–18787
41. O'Flaherty L, Adam J, Heather LC, Zhdanov AV, Chung YL, Miranda MX, Croft J, Olpin S, Clarke K, Pugh CW, Griffiths J, Papkovsky D, Ashrafian H, Ratcliffe PJ, Pollard PJ (2010) Dysregulation of hypoxia pathways in fumarate hydratase-deficient cells is independent of defective mitochondrial metabolism. Hum Mol Genet 19:3844–3851
42. Zhdanov AV, Favre C, O'Flaherty L, Adam J, O'Connor R, Pollard PJ, Papkovsky DB (2011) Comparative bioenergetic assessment of transformed cells using a cell energy budget platform. Integr Biol (Camb) 3:1135–1142
43. Ferrick DA, Neilson A, Beeson C (2008) Advances in measuring cellular bioenergetics using extracellular flux. Drug Discov Today 13:268–274
44. Hynes J, Natoli E, Jr, Will Y (2009) Fluorescent pH and oxygen probes of the assessment of mitochondrial toxicity in isolated mitochondria and whole cells. Curr Protoc Toxicol Chap. 2, Unit 2 16
45. Ashrafian H, O'Flaherty L, Adam J, Steeples V, Chung YL, East P, Vanharanta S, Lehtonen H, Nye E, Hatipoglu E, Miranda M, Howarth K, Shukla D, Troy H, Griffiths J, Spencer-Dene B, Yusuf M, Volpi E, Maxwell PH, Stamp G, Poulsom R, Pugh CW, Costa B, Bardella C, Di Renzo MF, Kotlikoff MI, Launonen V, Aaltonen L, El-Bahrawy M, Tomlinson I, Pollard PJ (2010) Expression profiling in progressive stages of fumarate-hydratase deficiency: the contribution of metabolic changes to tumorigenesis. Cancer Res 70:9153–9165

46. Wamelink MM, Struys EA, Jakobs C (2008) The biochemistry, metabolism and inherited defects of the pentose phosphate pathway: a review. J Inherit Metab Dis 31:703–717
47. Launonen V, Vierimaa O, Kiuru M, Isola J, Roth S, Pukkala E, Sistonen P, Herva R, Aaltonen LA (2001) Inherited susceptibility to uterine leiomyomas and renal cell cancer. Proc Natl Acad Sci U S A 98:3387–3392
48. Knox C, Sass E, Neupert W, Pines O (1998) Import into mitochondria, folding and retrograde movement of fumarase in yeast. J Biol Chem 273:25587–25593
49. Tomlinson IP, Alam NA, Rowan AJ, Barclay E, Jaeger EE, Kelsell D, Leigh I, Gorman P, Lamlum H, Rahman S, Roylance RR, Olpin S, Bevan S, Barker K, Hearle N, Houlston RS, Kiuru M, Lehtonen R, Karhu A, Vilkki S, Laiho P, Eklund C, Vierimaa O, Aittomaki K, Hietala M, Sistonen P, Paetau A, Salovaara R, Herva R, Launonen V, Aaltonen LA (2002) Germline mutations in FH predispose to dominantly inherited uterine fibroids, skin leiomyomata and papillary renal cell cancer. Nat Genet 30:406–410
50. http://www.ibidi.com/products/p_disposables.html
51. Zitova A, Cross M, Hernan R, Davenport J, Papkovsky DB (2009) Respirometric acute toxicity screening assay using Daphnia magna. Chem Ecol 25:217–227
52. Zitova A, O'Mahony FC, Cross M, Davenport J, Papkovsky DB (2009) Toxicological profiling of chemical and environmental samples using panels of test organisms and optical oxygen respirometry. Environ Toxicol 24:116–127
53. Schouest K, Zitova A, Spillane C, Papkovsky DB (2009) Toxicological assessment of chemicals using caenorhabditis elegant and optical oxygen respirometry. Environ Toxicol Chem 28:791–799
54. Zitova A, O'Mahony FC, Kurochkin IN, Papkovsky DB (2010) A simple screening assay for cholinesterase activity and inhibition based on optical oxygen detection. Anal Lett 43:1746–1755
55. Jezek P, Plecita-Hlavata L, Smolkova K, Rossignol R (2010) Distinctions and similarities of cell bioenergetics and the role of mitochondria in hypoxia, cancer, and embryonic development. Int J Biochem Cell Biol 42:604–622
56. Linsenmeier RA (1986) Effects of light and darkness on oxygen distribution and consumption in the cat retina. J Gen Physiol 88:521–542
57. Metzen E, Wolff M, Fandrey J, Jelkmann W (1995) Pericellular PO2 and O2 consumption in monolayer cell cultures. Respir Physiol 100:101–106
58. Rumsey WL, Schlosser C, Nuutinen EM, Robiolio M, Wilson DF (1990) Cellular energetics and the oxygen dependence of respiration in cardiac myocytes isolated from adult rat. J Biol Chem 265:15392–15402
59. Zhdanov AV, Ogurtsov VI, Taylor CT, Papkovsky DB (2010) Monitoring of cell oxygenation and responses to metabolic stimulation by intracellular oxygen sensing technique. Integr Biol 2:443–451
60. Bowman EJ, Siebers A, Altendorf K (1988) Bafilomycins: a class of inhibitors of membrane ATPases from microorganisms, animal cells, and plant cells. Proc Natl Acad Sci U S A 85:7972–7976
61. Teplova VV, Tonshin AA, Grigoriev PA, Saris NE, Salkinoja-Salonen MS (2007) Bafilomycin A1 is a potassium ionophore that impairs mitochondrial functions. J Bioenerg Biomembr 39:321–329
62. Schoonen WG, Stevenson JC, Westerink WM, Horbach GJ (2012) Cytotoxic effects of 109 reference compounds on rat H4IIE and human HepG2 hepatocytes. III: Mechanistic assays on oxygen consumption with MitoXpress and NAD(P)H production with Alamar Blue. Toxicol in Vitro 26:511–525
63. O'Riordan TC, Soini AE, Soini JT, Papkovsky DB (2002) Performance evaluation of the phosphorescent porphyrin label: solid-phase immunoassay of alpha-fetoprotein. Anal Chem 74:5845–5850
64. Kapellos GE, Alexiou TS, Payatakes AC (2007) A multiscale theoretical model for diffusive mass transfer in cellular biological media. Math Biosci 210:177–237

http://www.springer.com/978-3-0348-0524-7

Phosphorescent Oxygen-Sensitive Probes

Papkovsky, D.; Zhdanov, A.V.; Fercher, A.; Dmitriev, R.I.; Hynes, J.

2012, VIII, 101 p. 39 illus., 17 illus. in color., Softcover
ISBN: 978-3-0348-0524-7